Leading QCD corrections for indirect dark matter searches: A fresh look

Torsten Bringmann,[*] Ahmad J. Galea,[†] and Parampreet Walia[‡]

Department of Physics, University of Oslo, Box 1048, NO-0371 Oslo, Norway

The annihilation of nonrelativistic dark matter particles at tree level can be strongly enhanced by the radiation of an additional gauge boson. This is particularly true for the helicity-suppressed annihilation of Majorana particles, like neutralinos, into fermion pairs. Surprisingly, and despite the potentially large effect due to the strong coupling, this has so far been studied in much less detail for the internal bremsstrahlung of gluons than for photons or electroweak gauge bosons. Here, we aim at bridging that gap by presenting a general analysis of neutralino annihilation into quark anti-quark pairs and a gluon, allowing e.g. for arbitrary neutralino compositions and keeping the leading quark mass dependence at all stages in the calculation. We find in some cases largely enhanced annihilation rates, especially for scenarios with squarks being close to degenerate in mass with the lightest neutralino, but also notable distortions in the associated antiproton and gamma-ray spectra. Both effects significantly impact limits from indirect searches for dark matter and are thus important to be taken into account in, e.g., global scans. For extensive scans, on the other hand, full calculations of QCD corrections are numerically typically too expensive to perform for each point in parameter space. We present here for the first time an efficient, numerically fast implementation of QCD corrections, extendable in a straightforward way to nonsupersymmetric models, which avoids computationally demanding full one-loop calculations or event generator runs and yet fully captures the leading effects relevant for indirect dark matter searches. In this context, we also present updated constraints on dark matter annihilation from cosmic-ray antiproton data. Finally, we comment on the impact of our results on relic density calculations.

I. INTRODUCTION

The CERN Large Hadron Collider (LHC), now restarted with higher luminosity and center-of-mass energies after the scheduled two years' shut-down, continues to probe and constrain the electroweak scale for physics beyond the Standard Model (BSM). One of the better motivated BSM frameworks, Supersymmetry (SUSY) [1] has received a lot of attention at the LHC. As such the parameter space for weak scale SUSY is becoming constrained, with minimalistic versions claimed excluded [2,3]. Given the strong theoretical case for SUSY, and the absence of compelling alternatives, this highlights the importance of moving beyond the simplest case, and considering less constrained but equally well motivated versions of the "Minimal Supersymmetric Standard Model" (MSSM), with more free parameters. Consequently, the community has seen a steadily increasing effort to study such models and their much richer phenomenology, especially in the context of global scans that perform a simultaneous statistical fit to all accounted-for data (for recent examples, see [4–8]).

While so far no direct indication for BSM physics has been found at the LHC, clear evidence is provided by the observation of dark matter (DM) in the Universe, if so far

only via its gravitational interactions [9]. In weak scale SUSY the lightest supersymmetric particle (LSP) provides an excellent candidate for DM [10]. The most often studied situation, which we will also consider here, is an LSP given by the lightest neutralino. In fact, this provides a very useful template for the much more general class of weakly interacting massive particles (WIMPs), which are characterized by an interaction cross section with Standard Model states in the right range to be a thermal relic that fully accounts for the observed DM abundance today [11]. Such WIMPs can be searched for not only at colliders, but also in direct detection experiments looking for the recoil off target nuclei in large underground detectors, or indirect searches looking for WIMP annihilation products in the observed astrophysical fluxes of gamma rays or charged cosmic rays like antiprotons. Both direct [12] and indirect [13,14] searches now start to place severe limits on the simplest WIMP models, which makes astrophysical searches for DM interactions a promising avenue for discovery of new physics that is complementary to searches at the LHC.

Within the MSSM there is the interesting possibility of coannihilating DM [15,16], in which the LSP and next-to-lightest supersymmetric particle (NLSP) are near degenerate in mass and (co)annihilations of the NLSP (and potentially other particles only slightly heavier than the NLSP) are the decisive processes to determine the DM relic abundance. Scenarios with almost degenerate *squark NLSPs*, in particular, tend to constitute blind spots in LHC searches: even

[*]torsten.bringmann@fys.uio.no
[†]ahmad.galea@fys.uio.no
[‡]p.s.walia@fys.uio.no

043529-1

if created with relatively high rates such NLSPs produce jets in their decay that are too soft to pass the cuts [17], thereby generally evading current bounds from direct squark searches (as long as other, heavier states are out of reach for the available energy and luminosity; though monojet searches may help to fill that gap [18] and in some models flavor violating stop decays may be enhanced [19–21]). For light first generation squarks, and to some extent second generation squarks, direct searches therefore provide a powerful complementary tool to test such scenarios [22,23]. Independent of generation, indirect searches are also very promising in this respect [24], the reason being that internal bremsstrahlung (IB) processes with an additional gluon in the final state can lift the well-known helicity suppression of zero velocity neutralino annihilation.

In this article we carefully investigate the general importance of gluon IB in the context of indirect DM searches, by calculating the leading QCD corrections to the process shown schematically in Fig. 1. We perform our calculations for general MSSM scenarios, allowing in particular for arbitrary neutralino compositions and keeping the full quark mass dependence for gluon IB, i.e. $\chi\chi \to \bar{q}qg$. For loop corrections to the process $\chi\chi \to \bar{q}q$, which contribute to radiative corrections of the total annihilation cross section at the same order in the strong coupling α_s, we adopt a simplified description that fully captures the leading effects but is considerably easier to implement and numerically much faster. While we focus here for definiteness on the MSSM, our method is sufficiently general to be applicable to any BSM model that contains colored new states close in mass to the DM particle. As an important application, this allows us to include QCD corrections in a both fast and relatively simple way even in extensive global scans. As we will see, this is particularly relevant for scenarios where parts of the parameter space contain "squarks" almost degenerate in mass with the DM particle.

This article is organized as follows. In Sec. II we discuss the annihilation of neutralinos into $\bar{q}q$ and $\bar{q}qg$ final states and sketch the calculational methods that are employed (technical details being deferred to Appendix A). Section III is concerned with the impact on indirect DM
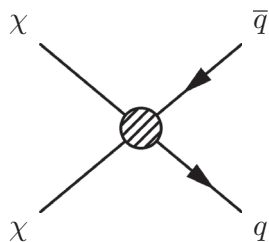

FIG. 1. Annihilation of neutralinos into $\bar{q}q$ from the point of view of an effective interaction. In this article, we focus on leading QCD corrections of this diagram that are relevant for indirect DM searches.

searches, including in particular a careful discussion of how DM induced cosmic-ray antiproton and gamma-ray spectra change by including $\bar{q}qg$ processes (for more details, see Appendix B). In Sec. IV we discuss the effect of gluon bremsstrahlung processes on relic abundance calculations in supersymmetric models. We present our conclusions in Sec. V.

II. NEUTRALINO ANNIHILATION INTO $\bar{q}qg$

We consider the minimal supersymmetric standard model (MSSM), where the four neutralinos are a linear combination of the superpartners of the neutral Higgs bosons and gauge fields,

$$\chi_i^0 = N_{i1}\tilde{B} + N_{i2}\tilde{W}^3 + N_{i3}\tilde{H}_1^0 + N_{i4}\tilde{H}_2^0. \tag{1}$$

Throughout, we will refer to the lightest of these Majorana fermions simply as *the* neutralino, $\chi \equiv \chi_1^0$. As schematically depicted in Fig. 1, we will be concerned with *nonrelativistic* neutralino annihilation to quarks (or, more specifically, with the *s*-wave part of the annihilation cross section). At tree level, more specifically, this process is determined by the contributions shown in Fig. 2: *s*-channel exchange of a Z or pseudoscalar Higgs boson, as well as *t*-channel squark exchange.

For nonrelativistic relative velocities v of the incoming DM particles, the annihilation cross section can be well approximated by expanding $\sigma v \simeq a_0 + a_1 v^2$. With Galactic velocities of $v \sim 10^{-3}$, annihilation in the Milky Way halo is thus typically dominated by *s*-wave contributions and given by $\sigma v \simeq a_0$. For Majorana DM the requirement that the annihilating pair be even under charge conjugation implies that the initial state in Figs. 1 and 2 transforms as a pseudoscalar under Lorentz transformations in the $v \to 0$ limit (0^{-+} in J^{PC} notation, see e.g. Ref. [25] for a recent comprehensive discussion). This requirement causes *s*-wave annihilations into $\bar{q}q$ to become helicity suppressed, scaling as $\sigma v \propto m_q^2/m_\chi^2$.[1] As first noted in Refs. [26,27], the helicity suppression can be lifted by radiating a gauge boson from an internal propagator (hence later coined "virtual" internal bremsstrahlung [28], VIB). The resulting enhancement of the annihilation rate is maximal for a *t*-channel particle degenerate in mass with the neutralino, $\sigma_{3\,\text{body}}/\sigma_{2\,\text{body}} \sim (\alpha_{\text{em}}/\pi)m_\chi^2/m_q^2$, and becomes suppressed by a factor of roughly 2 (3) for a mass difference of 10% (20%) [29]. Subsequently, the impact of IB was studied in great detail for both photons

---

[1]Note that the pseudoscalar A mixes left- and right-handed quarks, so for the *s*- channel exchange of A in Fig. 2, the *s*-wave is *not* actually helicity-suppressed. The Yukawa-coupling, however, results in the same parametric suppression $\sigma v \propto m_q^2/m_\chi^2$. A corresponding argument can be made for those contributions to the *t*-channel diagram that arise from the mixing of left- and right-handed squarks.
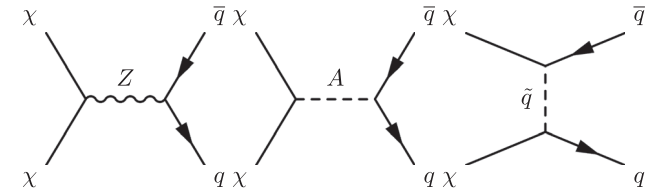
FIG. 2. s-wave neutralino annihilation into quark antiquark pairs proceeds through Z boson, pseudoscalar Higgs A and squark $\tilde{q}$ exchange.
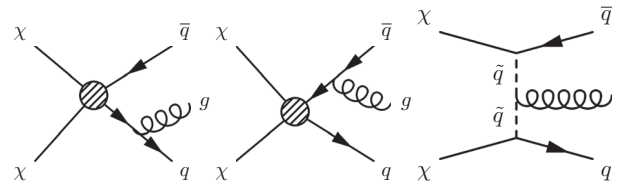

FIG. 3. Gluon internal bremsstrahlung, left to right: final state radiation, FSR, off q, off $\bar{q}$ and virtual internal bremsstrahlung, VIB. See Appendices A and B for a proper, and manifestly gauge-invariant, description of this naive distinction between FSR and VIB.
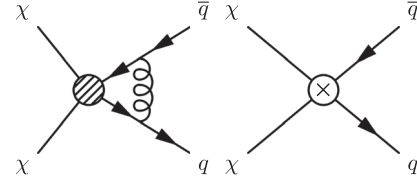
[28–38] and electroweak gauge bosons [39–50]. Given the nature of strong interactions, one should expect the effect to be even more pronounced for gluon internal bremsstrahlung in the case of quark final states, $\chi\chi \to \bar{q}qg$. Pictured in Fig. 3, however, this process has typically only been studied in the limit of $m_q \sim 0$ or for various simplifying assumptions concerning the neutralino composition and couplings (see, e.g., Refs. [23,24,51,52]). The purpose of this work is therefore to treat gluon IB more generally, in particular by allowing for arbitrary neutralino compositions and by considering heavier quarks.

The differential cross section for the process $\chi\chi \to \bar{f}f\gamma$, in the $v = 0$ limit, has been calculated in full generality in Ref. [28].[2] Accounting for the proper contraction of $SU(3)$ generators, the differential cross section for $\chi\chi \to \bar{q}qg$ is then readily obtained by the simple rescaling

$$Q^2\alpha_{\mathrm{em}} \to \frac{4}{3}\alpha_{\mathrm{s}}, \qquad (2)$$

where Q is the electric charge of the quark. For down-type quarks, we thus naively expect an effect of the order of $12\alpha_{\mathrm{s}}/\alpha_{\mathrm{em}} = \mathcal{O}(10^2)$ larger for gluon than for photon emission.[3] As a consequence, the *total* neutralino annihilation rate (including other final states than quarks) is also likely affected in a significant way. This should be contrasted to the much better studied case of QED, where light fermion final states typically contribute only subdominantly even when taking into account IB: rather than enhancing the total annihilation rate, the main phenomenological significance of *photon* VIB thus consists in the appearance of distinct spectral features in gamma rays and positrons, at $E \sim m_\chi$ [29,34]. In the QCD case this is different because of the expected size of the effect, but also because the additional final-state gluon will fragment with a high multiplicity into lower-energy particles, thus smearing out any spectral features potentially observable in cosmic rays (see however the discussion in Sec. III).

FIG. 4. (*Left*) 1-loop correction to Fig. 2, (*Right*) Sum of counterterm diagrams for all processes contributing to Fig. 2.

The need to calculate the total integrated, rather than only the differential cross section adds a complication because of the well-known infrared divergence associated to the emission of massless gauge bosons. This divergence is canceled by $\mathcal{O}(\alpha_s)$ interference terms between the diagrams in Fig. 2 and 1-loop corrections to the simplified tree-level process pictured in Fig. 1. More specifically the relevant diagrams are shown in Fig. 4, where the blob represents the sum over all processes in Fig. 2, and the cross represents the sum over all counterterms required to cancel ultraviolet (UV) divergences present in the left diagram of Fig. 4. As discussed in more detail in Appendix A, we will adopt a simplified model approach, where we *only* keep the terms corresponding to those diagrams. Compared to full next-to-leading (NLO) calculations at $\mathcal{O}(\alpha_s)$, see e.g. Refs. [54–57], this neglects diagrams containing gluinos and squark self-energies, as well as supersymmetric corrections to the quark self-energy and the neutralino-squark-quark coupling. These diagrams, however, are typically subdominant as none of them can lift the helicity suppression of the tree-level annihilation. Our simplified approach thus exactly reproduces the full NLO result in particular for SUSY models in which gluon bremsstrahlung processes are dominant. This is the generic situation for light quarks in the final state and squarks not much heavier than the neutralino.

III. INDIRECT DARK MATTER SEARCHES WITH GAMMA RAYS AND COSMIC-RAY ANTIPROTONS

In view of the small Galactic velocities, indirect searches for DM provide the ideal test bed for large effects on the

---

[2]The resulting expression is too long to be displayed here. It is, however, fully implemented in the publicly available DarkSUSY code [53] (see src/ib/dsIBffdxdy.f).

[3]In all calculations we evaluate α_s at the center of momentum energy $\sqrt{s}$ of the annihilating dark matter particles.

annihilation rate of neutralino DM in the zero velocity limit. In general, the final state quarks and gluons from DM annihilation in the Galactic halo will fragment and decay, and thereby eventually contribute to the observed flux in charged and neutral cosmic rays. Of special interest in this context are gamma rays [58], with very robust limits in particular provided by Fermi observations of dwarf spheroidal galaxies [13], and antiprotons which are produced in large quantities from the $\bar{q}qg$ final states we focus on here.

A. Energy spectrum from neutralino annihilation

We simulate parton showering and hadronization of $\bar{q}q$ and $\bar{q}qg$ final states using PYTHIA 8.2 [59,60], setting the center of momentum energy to be $2m_\chi$. For three-body final states, the resulting energy spectrum for photons and antiprotons dN/dT (with T denoting kinetic energy) is then derived by randomly sampling from the full gluon and quark energy distribution $d^2\tilde{N}_{\bar{q}qg}/dE_g dE_q$, obtained from Ref. [28] after rescaling as in Eq. (2) and with FSR processes subtracted to avoid double counting (for quantities we denote with a tilde, the FSR contribution is always understood to be subtracted; see Appendices A and B for details). To produce the expected spectra, we performed

10^7 PYTHIA runs for each quark channel, resulting in an accuracy of $\lesssim 1\%$ at the energies of interest.

For both antiproton and gamma ray spectra, there turns out to be substantial difference between $\bar{q}q$ and $\bar{q}qg$ final states; the main effect being that the fragmentation of the additional gluon in the final state significantly enhances the yields at small energies while slightly depleting it at higher energies (which indeed is expected as a result of the on average higher multiplicity in the final state). We illustrate this in Fig. 5, where we compare the spectra of antiprotons and photons resulting from $\bar{b}b$ and $\bar{b}bg$, and $\bar{u}u$ and $\bar{u}ug$ final states, for an assumed DM mass of $m_\chi = 100$ GeV. The high-energy feature visible in the $\bar{b}b$ spectra is a direct result of the decay of heavy b states such as B^0 mesons and is clearly absent in $\bar{u}u$ and $\bar{u}ug$ processes. For the displayed $\bar{q}qg$ final states, we choose the "maximal" VIB case, obtained for large squark mixing as defined by Eq. (B3). We found that this maximal VIB case leads to the largest possible difference between antiproton (or photon) spectra from $\bar{q}qg$ and $\bar{q}q$ final states, respectively.

The antiproton and gamma-ray spectra from $\bar{q}qg$ final states are in general model dependent, however, and therefore need to be determined on a model by model basis. This quickly becomes impractical, in particular when
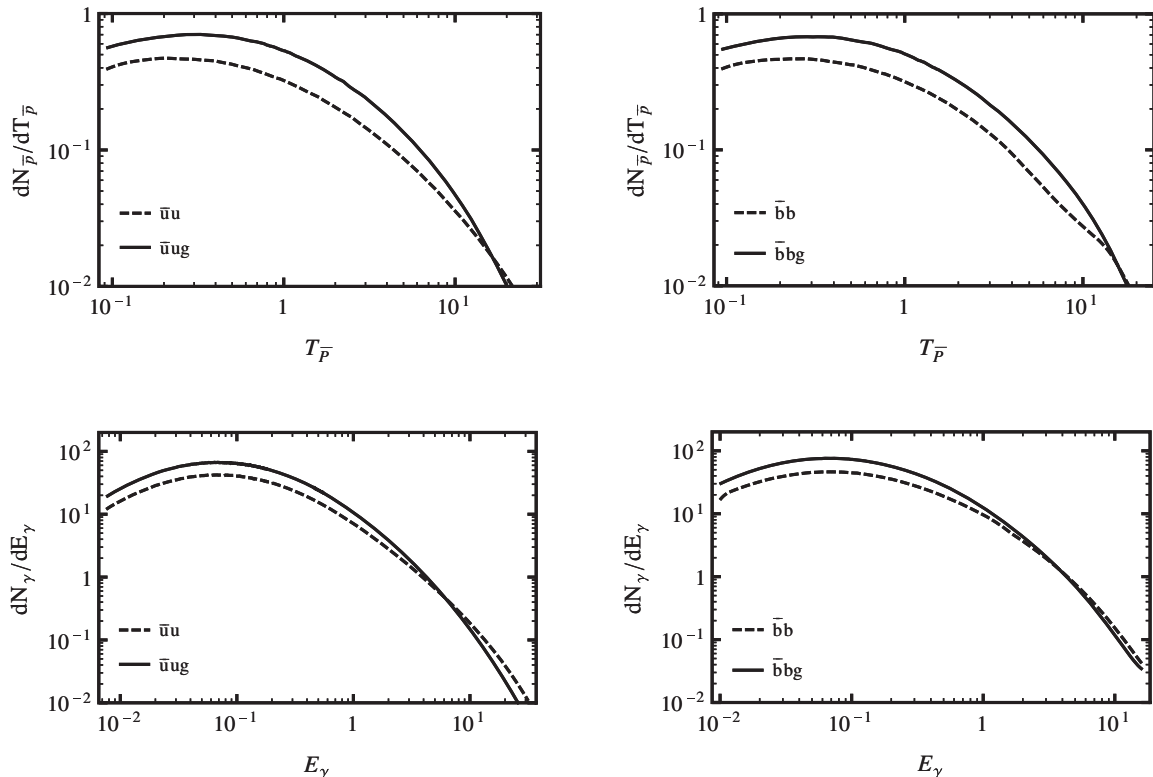

FIG. 5.   *Top panels.* Antiproton spectra from $\bar{q}q$ (dashed) and $\bar{q}qg$ (solid) for $m_\chi = 100$ GeV and both u (left) and b (right) quarks. For the 3-body case, a simplified gluon VIB distribution is assumed, with $m_\chi = m_{\tilde{b}}$ and vanishing squark mixing. *Bottom panels.* Same, but for photon spectra. All spectra are normalized such as to give the differential number N of antiprotons or photons per neutralino pair annihilation into 2-body or (FSR-subtracted) 3-body final states, respectively, cf. Eq. (B1). The high energy feature visible in the $\bar{b}b$ antiproton spectra is due to decaying B^0 mesons.

scanning over large numbers of models. Fortunately, we can circumvent this issue in an elegant way by approximating the full spectrum as the linear combination of the two extreme cases outlined in Appendix B, i.e. the $\bar{q}qg$ spectrum which is most different from $dN_{\bar{q}q}/dT$, given by the maximal VIB case already mentioned, and the $\bar{q}qg$ spectrum closest to $dN_{\bar{q}q}/dT$, the heavy sfermion limit given in Eq. (B7). Explicitly:

$$\frac{d\tilde{N}_{\bar{q}qg}}{dT_{\bar{p}}} \simeq y_{\bar{p}} \frac{d\tilde{N}_{\bar{q}qg}^{\text{VIB}}}{dT_{\bar{p}}} + (1 - y_{\bar{p}}) \frac{d\tilde{N}_{\bar{q}qg}^{m_{\bar{q}} \to \infty}}{dT_{\bar{p}}}, \qquad (3)$$

$$\frac{d\tilde{N}_{\bar{q}qg}}{dE_{\gamma}} \simeq y_{\gamma} \frac{d\tilde{N}_{\bar{q}qg}^{\text{VIB}}}{dE_{\gamma}} + (1 - y_{\gamma}) \frac{d\tilde{N}_{\bar{q}qg}^{m_{\bar{q}} \to \infty}}{dE_{\gamma}}, \qquad (4)$$

with $y_i \in [0, 1]$. If, on the other hand, the squarks are essentially unmixed, we interpolate instead between the extreme spectra obtained in that limit; i.e. we use Eqs. (B5) and (B8) rather than (B3) and (B7).[4] We established that this simple proscription indeed describes the real spectrum to an excellent precision, with the scaling parameter y only dependent on the likelihood that the gluon is emitted with a high energy. More precisely, we define

$$r \equiv \frac{r'_{\text{true}} - r'_{\tilde{m} \to \infty}}{r'_{\text{VIB}} - r'_{\tilde{m} \to \infty}}, \qquad (5)$$

where $r'_X = dN_{\bar{q}qg}^X(x_{\max})/dx_g$ and $x_{\max}$ maximizes the gluon energy spectrum. While somewhat arbitrary, r is a reasonable measure of the relative importance of the pure VIB and VIB/FSR mixing terms in the amplitude squared, which after the subtraction procedure described in detail in Appendix B, dominate the maximal VIB and heavy sfermion spectra respectively.

For a large set of randomized MSSM model parameters, and neutralino masses in the range from 10 GeV to 10 TeV, we then fit Eqs. (3) and (4) to the true 3-body antiproton or photon spectrum obtained from PYTHIA, using

$$\log_{10}(y) = \log_{10}(r) + \sum_i c_i r^{n_i}. \qquad (6)$$

The result for the parameters c_i and n_i are shown in Tables I and II. The contribution to the gluon energy spectrum from VIB/FSR mixing terms is proportional to the quark mass, and therefore expected to be suppressed relative to the purely VIB contribution for lighter quarks. In fact we find that in the mixed case for u and d quarks, and in the unmixed case for all quarks but the top, that $y(r) \simeq 1$ for

---

[4] As a criterion to distinguish between these two cases, we define $g_{\bar{q}_i}^r \equiv g_{\bar{q}_i q \chi}^R g_{\bar{q}_i q \chi}^L / (|g_{\bar{q}_i q \chi}^L|^2 + |g_{\bar{q}_i q \chi}^R|^2)$. If this quantity is *smaller* than 10^{-4} for a given SUSY model, we use the *unmixed* extreme spectra in the interpolation given by Eqs. (3) and (4).

TABLE I. Coefficients to obtain the antiproton spectrum from $\bar{q}qg$ final states for any MSSM model as a linear combination of "$m_{\bar{q}} \to \infty$" and "maximal VIB" $\bar{q}qg$ spectra for both large squark mixing ($g_{\bar{q}i}^r \geq 10^{-4}$, first three rows) and small squark mixing ($g_{\bar{q}i}^r < 10^{-4}$, last row). See Eqs. (3)–(6) for a full discussion. Note that the parameters c_i and n_i are, within the uncertainties discussed in the main text, independent of the neutralino mass for $10 \text{ GeV} \lesssim m_{\chi} \lesssim 10 \text{ TeV}$. For small squark mixing and all quarks lighter than t, the true spectrum is always well approximated by a pure VIB spectrum.

$\bar{q}q$	$g_{\bar{q}i}^r$	c_1	c_2	c_3	n_1	n_2	n_3
$\bar{c}c$	$\geq 10^{-4}$	-0.13	5.35	-5.22	0	9.8	9.15
$\bar{s}s$	$\geq 10^{-4}$	-0.4	-9.14	9.54	0	8.1	9.98
$\bar{t}t$	$\geq 10^{-4}$	-0.67	-2.41	3.08	0	0.43	0.27
$\bar{b}b$	$\geq 10^{-4}$	8.1	-8.32	0.22	0	0.02	9.53
$\bar{t}t$	$< 10^{-4}$	0.1	0.21	-0.31	0	8.73	5.53

$r \ll 0.1$ when fitting the antiproton/gamma-ray spectra. We therefore assume $y = 1$ in these cases for simplicity.

For the models tested this procedure was found to reproduce the true gamma-ray spectra from $\bar{q}qg$ to within 2% for $E_{\gamma} < 10^{-3}m_{\chi}$, 5% for $10^{-3}m_{\chi} < E_{\gamma} < 0.2m_{\chi}$ and within 8% for higher energies. For antiprotons the accuracy is within 10% for $T_{\bar{p}} < 10^{-2}m_{\chi}$, 8% for $10^{-2}m_{\chi} < T_{\bar{p}} < 0.2m_{\chi}$, and to within 20% for higher energies. We note that the relatively large deviation in particular at high energies is likely a result of models with intermediate squark mixings, i.e. $g_{\bar{q}i}^r \sim 10^{-4}$, which constitutes the worst point in both mixed and unmixed fits. In fact, for models away from the intermediate mixing region—corresponding to the bulk of models tested—the above errors are overly pessimistic, reducing to 3% for $10^{-3}m_{\chi} < E_{\gamma} < 0.2m_{\chi}$ and 5% for $10^{-2}m_{\chi} < T_{\bar{p}} < 0.2m_{\chi}$. As a possible future improvement on this procedure, one may use the values of the couplings to interpolate smoothly between the $g_{\bar{q}Lq\chi}^L = g_{\bar{q}Rq\chi}^R$ and $g_{\bar{q}Rq\chi}^L = g_{\bar{q}Rq\chi}^R = 0$ extreme spectra, thereby improving the fit at very high energies at the expense of introducing one more fitting parameter. Above $E_{\gamma}/T_{\bar{p}} \sim 0.5m_{\chi}$; furthermore, the reliability of simulated spectra decreases to around the 20% level due to the limited statistics of event generations, independent of the accuracy of the fit. The errors associated with the fit of

TABLE II. Same as Table I, but for gamma-ray spectra.

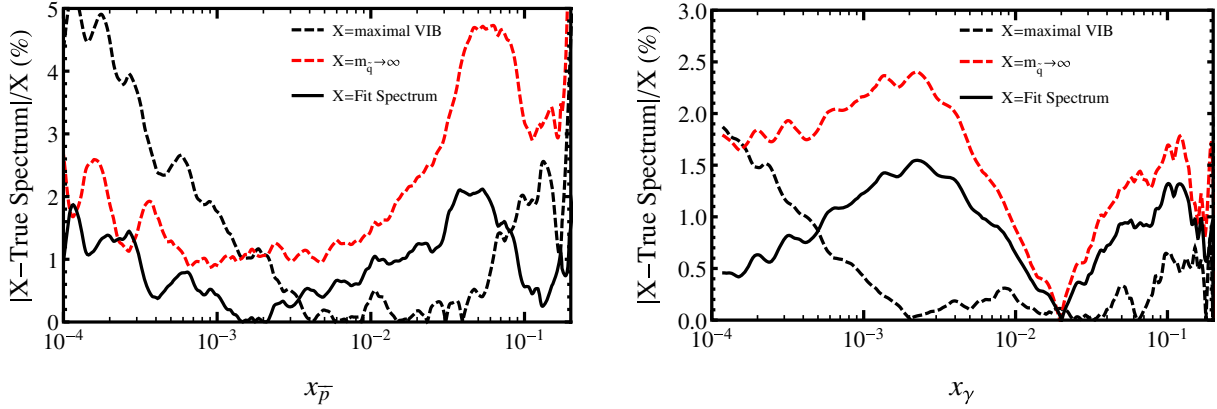| $\bar{q}q$	$g_{\bar{q}i}^r$	c_1	c_2	c_3	n_1	n_2	n_3
$\bar{c}c$	$\geq 10^{-4}$	0.03	-7.97	7.94	0	8.08	9.83
$\bar{s}s$	$\geq 10^{-4}$	0.12	-8.24	8.12	0	7.05	9.63
$\bar{t}t$	$\geq 10^{-4}$	-4.8	6.44	-1.64	0	0.06	0.34
$\bar{b}b$	$\geq 10^{-4}$	0.26	3.89	-4.15	0	2.22	1.63
$\bar{t}t$	$< 10^{-4}$	0.08	1.05	-1.13	0	8.36	7.45

FIG. 6.   Deviation from true antiproton (left) and gamma-ray (right) spectra for $\bar{b}bg$ VIB (dashed black), $\bar{b}bg\, m_{\tilde{q}} \to \infty$ (dashed red) and $\bar{b}bg$ fitted (solid black), coming from a pMSSM-7 model with parameters $M_1 = 2.95$ TeV, $M_2 = 4.96$ TeV, $\mu = 2.41$ TeV, $m_A = 10$ TeV, $\tan\beta = 14.77$, $A_t/M_1 = 1.218$ and $A_b/M_1 = 2.532$. This models features a mixed Higgsino-Bino lightest neutralino with mass $m_\chi = 2.49$ TeV and a relatively large sbottom mixing; both relic density and Higgs mass are consistent with observational constraints.

the function $y(r)$ itself are at worst of the order of 0.3; this results, by using Eqs. (3) and (4), in uncertainties in the spectra at the same order or smaller than the uncertainties discussed above. For illustration, we show in Fig. 6 the percent difference between a spectrum fitted using the above procedure and an MSSM model with a neutralino of mass 2.488 TeV, explicitly simulated for this particular model using PYTHIA.

We conclude this Section by stressing that the parameterization given in Eqs. (3)–(6) provides one of our main results. It allows us to compute antiproton and photon spectra from leading QCD corrections directly from tabulated "extreme" 3-body spectra—obtained in the heavy sfermion and maximal VIB limit, respectively—without having to run an event generator like PYTHIA for each model. As argued above, this is a highly desirable property in terms of computational performance which makes it very convenient for future applications, in particular in the context of large parameter scans. Our antiproton and gamma-ray yield routines, including the yield tables for gluon VIB and heavy sfermion IB, have been fully implemented in DarkSUSY [53] and will be available with the next public release. Concretely, we tabulated mixed/ unmixed VIB and $m_{\tilde{q}} \to \infty$ antiproton $d\tilde{N}_{\bar{q}qg}/dT_{\bar{p}}$ and gamma-ray spectra $d\tilde{N}_{\bar{q}qg}/dE_\gamma$ for all quarks, and for 100 dark matter masses in the range 5 GeV–10 TeV. For a given MSSM model, our numerical routines then interpolate the expected VIB and $\tilde{m} \to \infty$ spectra between the discrete values of neutralino masses explicitly simulated and weigh them according to Eqs. (3) and (4). Overall, this procedure reproduces the true antiproton/gamma ray spectrum to an accuracy better than $\sim$10% for $T_{\bar{p}}/E_\gamma < 0.2 m_\chi$, being as good as $\sim$3% in the energy range $10^{-3} m_\chi < T_{\bar{p}}/E_\gamma < 0.2 m_\chi$, as stipulated above.

B. Gamma-ray and antiproton constraints

While gamma rays propagate essentially unperturbed through the Galaxy, antiprotons are deflected by Galactic magnetic field inhomogeneities. The resulting motion can effectively be described as a random walk, and thus by a diffusion equation in momentum space [61]. In the following, we use the same prescription as adopted in Ref. [62] to derive limits on a dark matter annihilation signal in antiprotons. For the astrophysical background, we thus use a three-parameter model to take into account the effect of solar modulation via a freely varying force field parameter ϕ_F [63,64] and to interpolate between available extreme predictions obtained due to propagation model [65] and nuclear cross section uncertainties [66]. The antiproton flux from DM, on the other hand, depends to a much larger degree on the choice of propagation model than the astrophysical background; here, we use the recommended reference model, KRA, of the comprehensive analysis presented in Ref. [67]. Finally, we obtain limits on the signal by means of a likelihood ratio test [68] against the PAMELA data [69], where we profile over all parameters other than the signal normalization (noting that data from the AMS-02 experiment are still preliminary [70]). For further details of the procedure adopted, we refer the reader to Ref. [62]. In Fig. 7, we show the resulting limits on the annihilation rate into quark-antiquark pairs.[5]

In Fig. 8, we illustrate how these limits change when considering $\bar{q}qg$ rather than $\bar{q}q$ final states. Here, we adopt for illustration the mixed VIB spectrum for the case of $\bar{q}qg$

---

[5]These results differ slightly from the limits presented earlier [62]. The reason is that we use here PYTHIA 8.2, while the previous limits where derived using the fragmentation functions of DarkSUSY, which interpolates results obtained with PYTHIA 6.
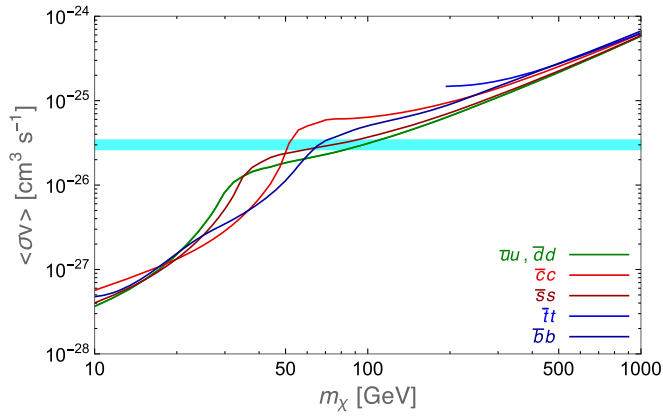
FIG. 7. Updated limits on the DM annihilation rate into quark pairs, derived from cosmic-ray antiproton data. The cyan area gives a rough indication of the cross section required for thermal DM production. See text for further details.
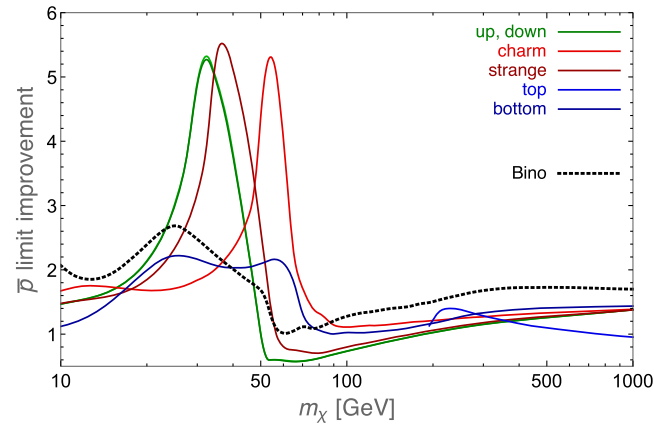

FIG. 8. Ratio of antiproton limits on the total annihilation rate σv into VIB $\bar{q}qg$ vs $\bar{q}q$ final states, as a function of the neutralino mass m_χ and assuming the *same cross section* for $\bar{q}qg$ and $\bar{q}q$. The actual improvement in the limits will thus be larger by a factor of up to about $(\alpha_{\rm s}/\pi)(m_\chi/m_q)^2$. Note that while the limits themselves (derived by the same procedure as adopted in Ref. [62]) strongly depend on the adopted propagation model, the displayed *ratios* are rather insensitive to this choice. The dotted line shows the case of a pure Bino and exactly degenerate squarks, see discussion after Eq. (7), as compared to a spectrum resulting from $\bar{b}b$ final states. Note that $\bar{q}qg$ final states are relevant in particular for squarks highly degenerate in mass with the neutralino; in such scenarios even neutralino masses well below 100 GeV can evade constraints from LEP [71,72] or the LHC [73,74].

final states, see Eq. (B3), with a normalization that corresponds to the *same* cross section for 3- and 2-body final states, i.e. $\tilde{\sigma}_{\bar{q}qg} = \sigma_0^{\rm full}$. The displayed improvement in the antiproton limits by a factor of up to ∼5 therefore results exclusively from the change in the antiproton spectrum; the *actual* limit improvement, for a given SUSY model, will be larger by another factor of up to $\tilde{\sigma}_{\bar{q}qg}/\sigma_0^{\rm full} \lesssim (\alpha_{\rm s}/\pi)(m_\chi/m_q)^2$. Let us stress that the displayed *ratios*

of limits are rather insensitive to the choice of propagation model (as opposed to the limits themselves, see Fig. 7). Taken together, this implies that gluon IB can indeed have a rather sizable impact on indirect searches for Majorana DM particles annihilating into quarks.

To further illustrate this, let us consider a pure Bino DM candidate with $m_b \ll m_{\tilde{B}} < m_t$ and all squarks exactly degenerate in mass $\tilde{B}$. The total annihilation cross section into all $\bar{q}qg$ final states is then given by [24]

$$\tilde{\sigma}_{\bar{q}qg}^{\rm Bino} v = \frac{\alpha_{\rm s}\alpha_Y^2}{m_{\tilde{B}}^2} \frac{565}{1944}(21 - 2\pi^2)$$

$$= 5.2 \times 10^{-27} \left(\frac{m_{\tilde{B}}}{100 \text{ GeV}}\right)^{-2} \text{cm}^3 \text{ s}^{-1}. \quad (7)$$

On top of that we also add the contribution from gluon pair final states [51,75]. Just as for single quark channels, the shape of the combined antiproton spectrum from Bino annihilation changes significantly when including QCD corrections. As indicated in Fig. 8, this improves antiproton limits by a factor of up to 2.7 compared to the "standard" spectrum resulting from $\bar{b}b$ final states. For the reference propagation model ("KRA"), we find that such a scenario can be excluded from antiproton data up to $m_{\tilde{B}} \sim 61$ GeV. Allowing a larger size of the diffusive halo, as realized in the "MAX" propagation model [76], even Bino and (exactly degenerate) squark masses below about 92 GeV would be excluded. Experiments with improved statistics, like AMS-02, will be even more sensitive to the spectral shape of the antiproton spectrum, and hence help to push these limits to even higher masses.

This clearly highlights the complementarity between indirect searches for DM and collider searches: While direct searches for squarks at the LHC have produced impressive limits reaching up to the TeV scale [73,77,78], it is crucial to remember that those limits do not apply to highly mass-degenerate scenarios. In fact, even first and second generation squarks with $m_{\tilde{q}} \lesssim 100$ GeV still remain unconstrained from such searches unless the squark to neutralino mass ratio is considerably higher than 10% [73]. Also earlier data from the large electron-positron collider (LEP) only constrain scenarios where the squarks are at least a few percent heavier than the neutralino [71]. Third generation squarks are typically even harder to probe, both at the LHC [74] and previously at LEP [72]. Below $m_\chi \sim m_Z/2 \sim 46$ GeV, contributions to the Z boson width typically provide the strongest constraints [79]; while independent of $m_{\tilde{q}}$, however, those limits still depend on the neutralino composition.

Similarly, *gamma-ray limits* are affected—even though, as discussed above, the spectra do not change as much as in the antiproton case. A full spectral analysis would in general depend on both the specific gamma-ray telescope and the form of the astrophysical backgrounds for the target
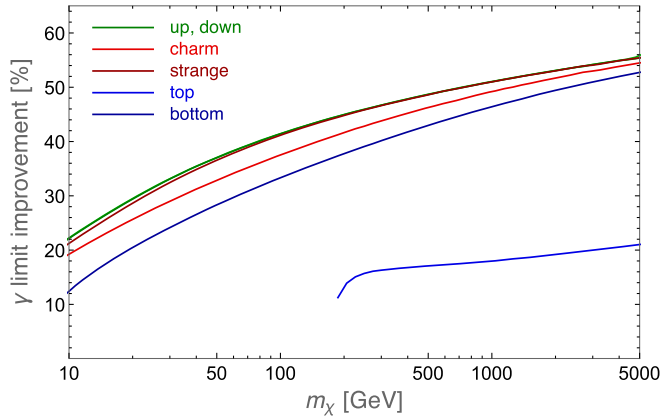
FIG. 9. Same as Fig. 8, but for gamma-ray limits obtained by comparing the photon count above 0.1 GeV. Also in this case the actual improvement in the limits will be larger by another factor of up to about $(\alpha_s/\pi)(m_\chi/m_q)^2$. Top quarks feature qualitatively different spectra compared to all other quarks, both for 2-body and 3-body final states, the reason being that top quarks are treated as decaying resonances in PYTHIA 8 (rather than as allowed final states).

in question, and hence be clearly beyond the scope of this work. For subdominant backgrounds, however, a very rough estimate of the effect can be obtained by simply comparing the integrated photon spectra from $\bar{q}qg$ and $\bar{q}q$ final states. As an illustrative example let us consider the photon count above 0.1 GeV, indicative of the lower energy threshold of the large area telescope (LAT) on board the Fermi satellite [80]. In Fig. 9, we show the ratio of this quantity for various quark final states. As anticipated, the enhancement is smaller than in the antiproton case. Still it is not negligible, in particular for large DM masses. The additional expected enhancement of $\tilde{\sigma}_{\bar{q}qg}/\sigma_0^{\text{full}} \lesssim (\alpha_s/\pi)(m_\chi/m_q)^2$, furthermore, is of course the same. This makes the QCD corrections computed here highly relevant also for gamma rays, the "golden channel" [58] of indirect DM searches.

IV. RELIC ABUNDANCE

As a second application to the leading radiative corrections we have computed here, we consider next the relic density of thermally produced neutralino dark matter. The standard method [81] to compute it, as implemented e.g. in DarkSUSY [53], is to solve the Boltzmann equation for the neutralino number density n_χ:

$$\partial_t n_\chi + 3H n_\chi = -\langle \sigma v \rangle_{\text{eff}} (n_\chi^2 - n_\chi^{\text{eq2}}).\qquad (8)$$

Here, H denotes the Hubble rate, $\langle \sigma v \rangle_{\text{eff}}$ the thermally averaged annihilation rate including coannihilations [15], and n_χ^{eq} the neutralino number density in thermal equilibrium. As before, we will use the simplified approach discussed in Appendix A to calculate the annihilation cross section for neutralinos. Concretely, we include the full QCD-corrected cross section $\sigma_{\text{tot}}^{\text{simp}}$ of the simplified model, cf. Eqs. (A17) and (A21), as well as the FSR-subtracted VIB cross section ($\tilde{\sigma}_{\bar{q}qg}$, see Appendix A 2) at zero velocity, and add them to the relic density routines of DarkSUSY.

For the computation of the neutralino relic density, it generally suffices to know $\langle \sigma v \rangle_{\text{eff}}$ at temperatures relatively close to chemical decoupling, i.e. $\langle \sigma v \rangle_{\text{eff}} \sim H n_\chi$ (unless one encounters complications, like in the case of the Sommerfeld effect for TeV neutralino masses [82–84]). For typical decoupling temperatures $T \sim m_\chi/25$, the second term in the nonrelativistic expansion of the neutralino annihilation rate,

$$\langle \sigma v \rangle \simeq a_0 + a_1 \langle v^2 \rangle + \cdots = a_0 + \frac{3a_1}{2}\frac{T}{m_\chi} + \cdots, \qquad (9)$$

typically becomes much larger than the first—at least for $\chi\chi \to \bar{f}f$ processes—and therefore sets the relic density. With the VIB corrections we have computed here, however, the first term is only parametrically suppressed by α_s/π rather than m_q^2/m_χ^2. This is almost of the same order as the $\langle v^2 \rangle$ suppression of the second term, so one would naively expect that including gluon VIB might change the relic density by up to 100% in extreme cases—which should be compared to the percent-level accuracy with which this quantity has been determined observationally [9].

As we will see in more detail below, however, there are two main obstacles to this naive expectation. The first one is that any relevant VIB enhancement would require rather high neutralino masses, $m_\chi \gg m_q/\sqrt{\alpha_s/\pi}$. In this case, both $\bar{t}t$ and electroweak gauge boson final states open up as possible final states; being typically not (sufficiently) suppressed, and thus not subject to large VIB enhancements, they will thus dominate the *total* annihilation rate. The second obstacle is that unsuppressed VIB rates require a small mass splitting between the neutralino and the squarks exchanged in the t-channel. In this situation, however, coannihilations [15] with those squarks need to be taken into account, and these contribute to $\langle \sigma v \rangle_{\text{eff}}$ with an unsuppressed contribution in the zero-velocity limit already at tree-level. In order to assess the impact of gluon VIB on the relic density, one therefore has to fully include these effects.

For the sake of simplifying the discussion, let us start by considering the case of a neutralino that is an almost pure Bino. If we furthermore ensure that both sleptons and the pseudoscalar Higgs are much heavier than the other states, neutralino annihilation into quark pairs via t-channel squark exchange dominates the total cross section. For such a scenario, the impact of QCD corrections on the relic density can thus be expected to be maximized. In Fig. 10, we show the resulting Ωh^2 as a function of m_χ, with all squark masses fixed to a common value of $m_{\tilde{q}} = 1.1 m_\chi$
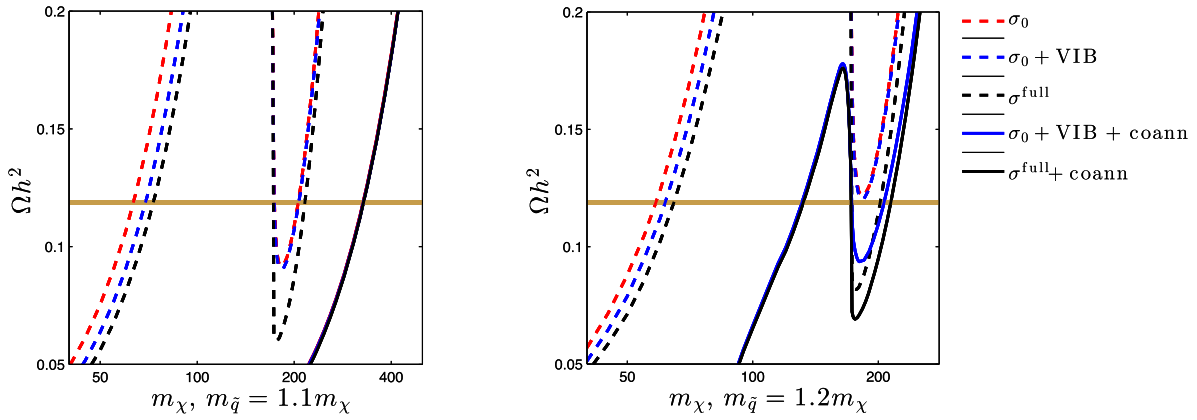
FIG. 10.   *Variation of Ωh^2 vs m_χ for a pure Bino model.* Left panel: common squark mass of $m_{\tilde{q}} = 1.1 m_\chi$, right panel: $m_{\tilde{q}} = 1.2 m_\chi$. The tree-level annihilation cross section is denoted by σ_0, while σ^{full} contains all relevant QCD corrections; this includes the simplified model NLO corrections contained in $\sigma_{\text{tot}}^{\text{simp}}$, cf. Eq. (A17), the VIB cross section $\tilde{\sigma}_{\tilde{q}qg}$ and the annihilation rate to two gluons. The brown band shows the 1σ limits on the DM density as observed by the Planck Collaboration [9]. For smaller m_χ, the dominant impact of the QCD corrections studied here is due to the VIB contributions, though gluon pair production plays an almost equal role. Near the top threshold, the dominant change is instead related to the simplified model NLO corrections to the two-body rate. For $m_{\tilde{q}} \lesssim 1.1 m_\chi$, both contributions are negligible compared to the impact of squark coannihilations.

(left panel) or $m_{\tilde{q}} = 1.2 m_\chi$ (right panel), along with the measured value $\Omega h^2 \sim 0.1188 \pm 0.0010$ [9]. Solid (dashed) lines indicate the relic density with (without) taking into account coannihilations. We separately show the result for the tree-level cross section σ^0 and adding only the VIB part $\tilde{\sigma}_{\tilde{q}qg}$, as well as for the full QCD-corrected annihilation cross section σ^{full}. In the latter, we include here not only the $\mathcal{O}(\alpha_s)$ corrections discussed in Appendix A 1 ($\sigma_{\text{tot}}^{\text{simp}}$) but also the $\mathcal{O}(\alpha_s^2)$ process of neutralino annihilation into a gluon pair [51,75], which is unsuppressed in the zero-velocity limit and already implemented in DarkSUSY.

In the figure, we can clearly identify three regions of interest for the relic density and the active channels of annihilation. Firstly, for neutralino masses less than the top mass, annihilation takes place only into lighter quarks (u, d, s, c and b). Secondly, for neutralino masses above the top threshold. And lastly, when the relic density actually becomes equal to the observed DM density, after fully taking into account coannihilations (neutralino-squark and squark-squark). In the first region, the dominant change in relic density (when assuming no coannihilations) is due to VIB, with all allowed quark channels contributing equally for $m_q \ll m_\chi$. For $m_{\tilde{q}} = 1.1 m_\chi$ this results in a decrease in Ωh^2 by about 15%, as compared to the tree-level result that would require a neutralino with $m_\chi = 63.4$ GeV[6]; this can

be compensated by increasing m_χ by 9% (from 63.4 to 69.1 GeV). For heavier squarks the VIB contributions become as expected less important, and $\chi\chi \to gg$ starts to dominate the annihilation rate. Once we cross the top-threshold, the unsuppressed annihilation into top quarks ($\sigma_{\bar{t}t}^0 \propto m_t^2/m_\chi^2$) causes a strong increase in the cross section and thus a decrease in the relic density. With the neutralino being only slightly heavier than the top, we cannot expect any sizeable VIB enhancement. Annihilation into gluon pairs is no longer important, either. Instead, the dominant QCD effect in this regime is due to NLO corrections to the simplified model cross section, and the resulting drop in the relic density is consistent with the enhancement of the s-wave part of $\langle \sigma v \rangle$ by the factor $\sigma_{\text{tot}}^{\text{simp}}/\sigma_0^{\text{simp}}$ shown in Fig. 15. Note that this cross section enhancement is independent of the squark mass, so we observe the same drop in the relic density in both panels of Fig. 10. For much heavier neutralinos, on the other hand, $\sigma_{\text{tot}}^{\text{simp}}$ needs to be resummed as in Eq. (A21) and would become smaller than σ_0^{simp}, see again Fig. 15, hence increasing Ωh^2.

As also becomes clear from the left panel of Fig. 10, however, coannihilations in the presence of very light squarks vastly dominate over annihilation processes, implying that QCD corrections to the latter have no impact on the relic density. Increasing the squark mass, on the other hand, decreases the effect of coannihilations and therefore lowers the value of m_χ that results in the observed relic density. For a common squark mass of $m_{\tilde{q}} \gtrsim 1.2 m_\chi$, and for neutralino masses just above the top threshold, the NLO corrections contained in $\sigma_{\text{tot}}^{\text{simp}}$ then start to dominate over the coannihilations (see the right panel of Fig. 10). This causes a decrease in the relic density by up to about

---

[6]Note that this actually corresponds to the *expected* order of magnitude for the enhancement in the annihilation rate: following the discussion after Eq. (9), the maximally possible increase would naively be about $(\alpha_s/\pi)/(3/2/25) \sim 60\%$; this expectation however, should be lowered by a factor of ~ 2 because of the nondegenerate squark mass, and slightly further due to the finite quark masses.
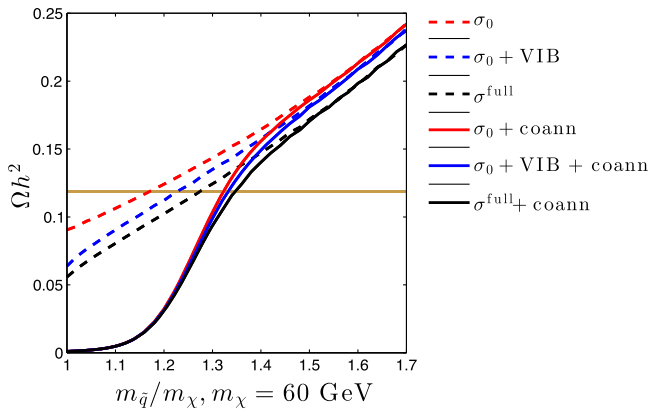
FIG. 11. Comparison of the resulting Ωh^2 when excluding/including coannihilations and excluding/including QCD corrections. For this plot, we again assume the neutralino to be a pure Bino, but fix its mass to $m_\chi = 60$ GeV; line styles are the same as in Fig. 10. Both VIB and gluon pair production enhance the tree-level annihilation rate significantly, the latter being less suppressed by higher squark masses, but this hardly affects the relic density when taking into account coannihilations.

FIG. 12. The squark to neutralino mass ratio $m_{\tilde{q}}/m_\chi$ that results in $\Omega h^2 \sim 0.12$, for a given neutralino mass m_χ, when assuming a pure Bino annihilating only into quarks. Line styles are again the same as in Fig. 10. Considering only annihilations, VIB corrections have a larger impact on the relic density than gluon pair production for $m_{\tilde{q}} \lesssim 1.2 m_\chi$. In this range, however, the most important contribution comes from the coannihilations $\chi \tilde{q}_i \to W^\pm q_j$, $q_i g$ and $\tilde{q}_i \tilde{q}_i^* \to gg$. The peak centered at $m_\chi \sim 70$ GeV is due to the resonant top production in the process, $\chi \tilde{t} \to t^* \to W^\pm b$. For lower neutralino masses, both VIB and gluon pair production have a visible, if small, impact on the relic density.

12%, significantly greater than the observational uncertainty in Ωh^2.

Increasing the squark mass even further reduces the contributions from squark coannihilations down to the point where annihilations into light quarks, and thus potentially VIB corrections, become decisive in setting the correct relic density. As illustrated in Fig. 11 for a fixed neutralino mass of 60 GeV, however, this only happens for squark masses where also the VIB corrections are so suppressed that their effect on the relic density becomes much less visible: for $m_{\tilde{q}}/m_\chi \lesssim 1.5$, VIB corrections have an increasingly larger impact on neutralino annihilation, but coannihilation processes quickly start to contribute even stronger to $\langle \sigma v \rangle$; for $m_{\tilde{q}}/m_\chi \gtrsim 1.5$, on the other hand, neither effect is sizeable. The contribution from $\chi\chi \to gg$ to the annihilation rate, on the other hand, is equally important for most values of the squark masses and is comparable in size to the VIB contribution for $m_{\tilde{q}}/m_\chi \lesssim 1.2$. As a result, gluon pair production has a visible effect on the relic density for $m_{\tilde{q}}/m_\chi \gtrsim 1.3$.

The same point is also illustrated in Fig. 12, which shows the $m_{\tilde{q}}/m_\chi$ ratio required for neutralino masses below the top threshold to give the observed relic density. For small m_χ the total annihilation rate is large, and we have to require high values of $m_{\tilde{q}}$ to bring the cross section into the desired range. Decreasing the squark mass, one starts to see some impact of VIB corrections on the relic density (including coannihilations) from around $m_{\tilde{q}}/m_\chi \lesssim 1.4$. Those corrections change the relic density by up to about 5%; while this may sound like a small effect, recall that it is well beyond the experimental uncertainty in the observed DM density. In this mass region, the contribution from
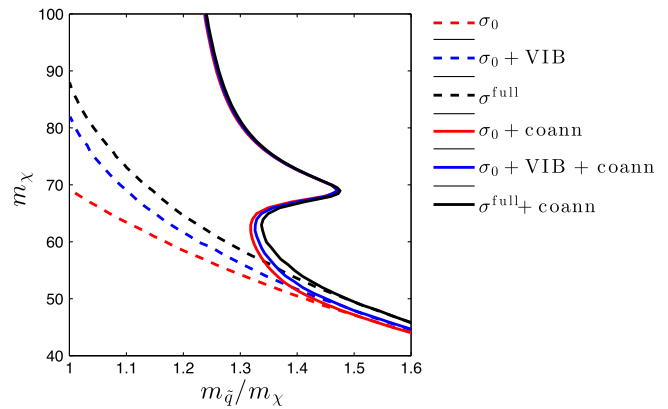
$\chi\chi \to gg$ is actually even somewhat larger. For higher neutralino masses, or smaller squark masses, the coannihilation processes $\chi \tilde{q}_i \to W^\pm q_j$, $q_i g$ and $\tilde{q}_i \tilde{q}_i^* \to gg$ then start to greatly increase $\langle \sigma v \rangle$, thus rendering all annihilation processes insignificant.

From the above discussion we conclude that, for Bino-like neutralinos lighter than the top quark the relic density (considering only annihilations) can be visibly decreased by including gluon VIB in the total annihilation rate—but this effect is inevitably washed out due to the unsuppressed coannihilations, apart from a small squark mass window around $m_{\tilde{q}} \sim 1.4 m_\chi$. Near top-threshold we see a significant decrease in the relic density due to the virtual loop corrections, $\sigma_{\rm tot}^{\rm simp}$, an effect which is independent of both coannihilations and VIB. It is worth noting that the above analysis considered the most optimal situation in terms of maximizing the effect of VIB corrections on the relic density. Opening up further channels, e.g. by decreasing any of the other sparticle masses or by allowing small Wino or Higgsino contributions to the neutralino composition, would further decrease the relative contribution from the quark final states and thus the effect of QCD corrections. For example, setting *all* sfermion masses to be equal would shift the annihilation lines below the top threshold in Fig. 10 by about $m_\chi \to 1.8 m_\chi$ due to the different couplings (hypercharges) of squarks and sleptons to a Bino; this is sufficient to completely hide even the small VIB effects one could potentially see in this region of parameter space (cf. the $m_\chi \sim 60$ GeV region in Fig. 12).

Let us use the remainder of this section to put these general findings in the context of previous work and concrete scenarios. The impact of QCD corrections to neutralino annihilation on the relic density has been studied by various authors [27,51,54–56,85–88]. An extensive study for annihilation into quark final states including all diagrams at $\mathcal{O}(\alpha_s)$, in particular, was performed by Herrmann *et al.* [54]. Here, the focus was on models with neutralinos close to the top threshold where, as noted above, the dominant correction is due to virtual loop corrections. A detailed comparison between our simplified approach and theirs is provided in Appendix A 4.

As also discussed above, coannihilations can increase the total annihilation rate significantly and thereby open up new regions of parameter space for SUSY models for which the relic density otherwise would be too large. Models with squark masses close to the neutralino mass, in particular, can be realized in many extensions of SUSY. For example in cMSSM models, squarks become light when the sfermion mass $m_{1/2}$, is lighter than the common gaugino mass m_0 and the CP-odd Higgs A is very heavy, $m_A \gg m_\chi$, which increases the squark mixing [89]. We can further increase the parameter space for such coannihilation scenarios if we consider less constrained models. For example Ref. [54] uses nonuniversal Higgs and gaugino mass models. Another way is to specify the parameters at a lower energy scale (pMSSM models) with the $U(1)$ gaugino mass parameter close to the squark mass, i.e. $M_1 \lesssim m_{\tilde{q}}$.

Due to experimental and phenomenological constraints, typically only coannihilation with top squarks is allowed for the most constrained models and thus is of particular interest (for a detailed discussion see [90]). The *stop coannihilation strip* in the cMSSM, for example, has been studied in much detail by many authors [91–101], with new limits resulting in particular after the discovery [102,103] of the Higgs boson. It extends up to neutralino masses of $m_\chi \sim 6500$ GeV [100] and is as already mentioned realized for very large values of m_A (increasing this parameter even further would lead to $m_{\tilde{t}} < m_\chi$, rendering the model unphysical). For such large neutralino masses, VIB processes start to dominate neutralino annihilation; in agreement with our previous estimate, we find that $\tilde{\sigma}_{\tilde{t}tg}$ becomes equal to $\sigma_{\tilde{t}t}$ at around $m_\chi \sim 2$ TeV. As indicated by the name, however, the by far largest contribution to the total effective annihilation rate in these scenarios comes from *coannihilations*, through $\tilde{t}\chi \to tg$ and $\tilde{t}\tilde{t} \to gg$, rather than from annihilation processes [85,104]. Due to the colored initial states, these and other coannihilation processes receive sizable QCD corrections; those have been studied in some detail [105–109] and been found to affect the relic density at a level that exceeds the experimental uncertainty.

Concerning first and second generation squarks, both ATLAS [73,77] and CMS [78] Collaborations report a mass limit of about 850 GeV from generic squark searches, i.e. following a simplified model approach, when assuming all eight squarks to be degenerate in mass; if all but one of these squarks is in the TeV range, the mass limit on the lightest squark is only about 450 GeV. As mentioned earlier, however, these limits do not apply for squarks highly degenerate in mass with the neutralino; mass differences below 20 GeV [78] or a few GeV [77] remain generally unconstrained. In particular for neutralino and squark masses around roughly 100 GeV, this leaves an intriguing unconstrained window [73] with interesting model-building options in nonminimal SUSY scenarios. As discussed in Sec. III, the large VIB contributions in such scenarios become a powerful probe for indirect DM searches. The relic density, on the other hand, is mostly set by coannihilations and thus not noticeably affected by this kind of QCD corrections.

V. CONCLUSIONS

Cosmological and astrophysical measurements have reached an impressive level of precision in recent years, calling for a match in terms of equally precise theoretical predictions. With this in mind, we have presented a comprehensive study of the impact of QCD radiative corrections to DM annihilations, focusing on supersymmetric neutralinos.

We find that QCD corrections can indeed very strongly affect the interpretation of indirect DM searches, due to two unrelated effects: i) an *enhancement* of the helicity-suppressed tree-level cross section by a factor of about $(\alpha_s/\pi)(m_\chi/m_q)^2$, in the limit of vanishing relative velocity, and ii) a significant *change in the spectrum* of the messengers of indirect detection, like gamma rays and cosmic-ray antiprotons (see Figs. 8 and 9). While briefly mentioned in Ref. [24], in particular the second point has never been addressed in detail before. We also provided updated antiproton limits on DM annihilating into quarks (Fig. 7) and pointed out that the large enhancements of the annihilation rate just mentioned makes indirect searches complementary to a blind spot of collider searches for new physics, namely scenarios where the squarks are almost identical in mass to the DM particle. The impact of the QCD corrections to neutralino annihilation studied here on the *relic density*, on the other hand, is much smaller because coannihilations typically dominate. Still, in certain parameter regions these corrections can clearly affect the relic density beyond the level of precision set by current observations (see, e.g., Figs. 10 and 12).

Maybe most importantly, we have presented a fast and efficient way of numerically implementing leading QCD corrections. This method fully captures the above mentioned effects and is in principal extendable in a straightforward way also to nonsupersymmetric models. In particular, we have modeled the annihilating neutralino pair as a decaying pseudoscalar with additional dimension-5 and 6 operators—see Eqs. (A1) and (A11) and the discussion in Appendix A—and approximated the resulting

cosmic-ray spectra for a given model as a simple interpolation between the possible extreme cases, see Eqs. (3) and (4) and the discussion in Appendix B. We also corrected the effective way in which most current computer codes, like DarkSUSY [53] or micrOMEGAs [110], handle QCD corrections to the decay of neutralinos (see the discussion in Appendix A 3). This makes both calculations of the relic density and present annihilation rates more reliable, in particular for light quark final states.

Our implementation allows us to take into account the leading effects of QCD corrections, especially for indirect DM searches, without the need for numerically expensive full one-loop evaluations or extensive runs of event generators. This leads to a significant gain in performance, which is highly attractive for global scans of high-dimensional parameter spaces, where too time-consuming calculations of relevant observables typically constitute a serious bottleneck. The traditional standard example for the latter are relic density calculations that fully take into account coannihilations; the most important example in the context of indirect detection, on the other hand, is given by the highly model-dependent cosmic-ray spectra that result when taking into account radiative corrections (see also Refs. [50,111]). In this sense, our approach is therefore complementary to that of packages like DM@NLO [112] which aim at full NLO calculations, and hence even higher precision (unless the leading-log resummation that we take fully into account dominates), at the expense of the time required to compute observables for a given model. Another advantage of our method is that we provide the annihilation cross section directly in the limit of vanishing relative velocity, which in most cases is the relevant quantity for indirect DM searches but which presently cannot be provided by DM@NLO. All necessary numerical routines will be included in the next public release of DarkSUSY.

APPENDIX A: EFFECTIVE TREATMENT OF NEUTRALINO ANNIHILATION

The full calculation of the NLO neutralino cross section can be computationally time consuming, though can be simplified substantially by taking advantage of the majorana nature of the dark matter pair: for small relative velocities, we can approximate the annihilating neutralino pair as the effective decay of a pseudoscalar boson. In Sec. A 1 we discuss this simplified model and describe its implementation. In Secs. A 2 and A 3 we perform the calculation of decays within the simplified model at next to leading order in α_s, while keeping the full expressions for gluon IB, and finally in Sec. A 4 we discuss the error associated with using this paradigm to describe neutralino annihilation.

1. Approximating annihilation as pseudoscalar decay

As discussed briefly in Sec. II, a pair of nonrelativistic Majorana neutralinos transforms to an excellent approximation as a pseudoscalar under Lorentz transformations. Practically this means that the initial state fermion bilinear in the amplitude can be replaced with the s-wave projector $P_{S_0} = \frac{\gamma^5}{\sqrt{2}}(m_\chi - p\!\!\!/ /2)$, where m_χ is the neutralino mass and p is the total momentum of the system (see, e.g., Ref. [114]). Assuming no CP-violating interactions, the tree-level amplitude for $\chi\chi \to \bar{q}q$ thus reduces to the same form as that of a decaying pseudoscalar ϕ with mass $M = 2m_\chi$,[7] up to a conventional constant normalization factor A of mass dimension one, with an interaction Lagrangian given by

$$\mathcal{L}_{\text{int}}^{\text{simp}} = -g_p \phi \bar{q} i \gamma^5 q - \frac{1}{\Lambda_a} \partial_\mu \phi \bar{q} \gamma^\mu \gamma^5 q. \quad (A1)$$

Here, g_p is an effective pseudoscalar coupling, and Λ_a is an effective axial-vector coupling with mass dimension one. This leads to a squared matrix element of

$$|\mathcal{M}|^2 = 2M^2 \left(g_p + \frac{2m_q}{\Lambda_a}\right)^2. \quad (A2)$$

The same result, divided by A^2, is obtained in the case of annihilation, implying the following relation between the total quark production rate in this simplified model Γ_0^{simp} and the total tree level neutralino cross section σ_0^{full}:

$$\Gamma_0^{\text{simp}} = A^2 m_\chi \sigma_0^{\text{full}} v. \quad (A3)$$

---

[7]In the interest of simplifying the presentation, we have here taken the limit of vanishing relative velocity v of the annihilating neutralinos. However, given that different partial wave contributions cannot mix, the entire discussion of Appendix A is valid not only in the $v = 0$ limit; rather, the *full s-wave part* of the cross section takes, at tree-level, the same form as a decaying pseudoscalar with mass $M = \sqrt{s}$. In order to take into account the full velocity dependence of the s-wave, one therefore simply has to replace $m_\chi \to \sqrt{s}/2$ in every expression of the Appendix that involves the neutralino mass.
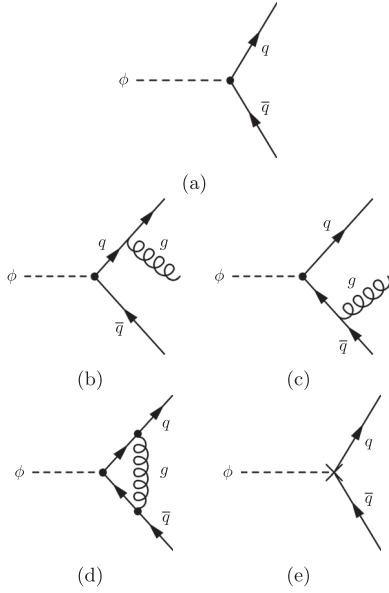
FIG. 13. Diagrams contributing to pseudoscalar decay up to $\mathcal{O}(\alpha_s)$: (a) Tree level decay, (b) FSR off of q, (c) FSR off of $\bar{q}$, (d) 1-loop vertex correction, (e) counterterm diagram.

From here on the superscript "simp" stands for calculations done in the simplified model and implicitly includes contributions from all operators in Eq. (A1).

In the interest of relating the full cross section $\sigma_{\rm tot}^{\rm full}$ at NLO to the decay rate of our simplified model, we will now generalize Eq. (A3) to an arbitrary subprocess X, and *define* an annihilation rate $\sigma_X^{\rm simp} v$ by the corresponding decay rate in the simplified model,

$$\sigma_X^{\rm simp} v \equiv \frac{\Gamma_X^{\rm simp}}{A^2 m_\chi}. \tag{A4}$$

At tree level ($X = 0$), we thus have $\sigma_0^{\rm simp} = \sigma_0^{\rm full}$ by construction, but in general one expects $\sigma_X^{\rm simp} \neq \sigma_X^{\rm full}$ (note, however, that the dependence of $\sigma^{\rm simp}$ on the conventional factor A always cancels). In general $\sigma_X^{\rm simp}$ does thus not constitute a physical cross section, but is simply a useful device for comparing the simplified model to the full neutralino cross section.

Henceforth we will denote vertex corrections by $X = V$, counterterms by $X = C$ and gluon internal bremsstrahlung by $X = B$. The diagrams for the contributing processes in the simplified model are pictured in Fig. 13: the cross section up to order α_s is given by the sum of tree level and bremsstrahlung cross sections, $\sigma_0^{\rm simp}$ and $\sigma_B^{\rm simp}$, plus the interference between tree level and vertex correction ($\sigma_V^{\rm simp}$) as well as counterterms ($\sigma_C^{\rm simp}$). For the full model, we thus have

$$
\begin{aligned}
\sigma_{\rm tot}^{\rm full} &= \sigma_0^{\rm full} + \sigma_B^{\rm full} + \sigma_V^{\rm full} + \sigma_C^{\rm full} + \sigma_\star^{\rm full} \\
&= \sigma_{\rm tot}^{\rm simp} + (\sigma_{\rm tot}^{\rm full} - \sigma_{\rm tot}^{\rm simp}) \\
&= \sigma_{\rm tot}^{\rm simp} + \tilde{\sigma}_{\bar{q}qg} + \sigma_{\rm Error}
\end{aligned}
\tag{A5}
$$

where $\sigma_\star^{\rm full}$ denotes interference terms between the tree-level result and additional diagrams not present in the simplified model,[8] and

$$\sigma_{\rm Error} \equiv (\sigma_V^{\rm full} - \sigma_V^{\rm simp}) + (\sigma_C^{\rm full} - \sigma_C^{\rm simp}) + \sigma_\star^{\rm full}. \tag{A6}$$

In the final step, we also have introduced the *FSR subtracted 3-body cross section*[9]

$$\tilde{\sigma}_{\bar{q}qg} \equiv (\sigma_B^{\rm full} - \sigma_B^{\rm simp}). \tag{A7}$$

The calculation of the full NLO cross section can thus be broken up into two pieces, the model independent $\sigma_{\rm tot}^{\rm simp}$, which we calculate analytically in Sec. A 3, and the just introduced quantity $\tilde{\sigma}_{\bar{q}qg}$ which, as we discuss next, contains potentially large corrections due to lifting the helicity suppression of $\sigma_0^{\rm full}$. The error in using the simplified model, $\sigma_{\rm Error}$, is in general model dependent but expected to be small, and will be discussed further in Sec. A 4.

2. Internal bremsstrahlung

In the simplified model, internal bremsstrahlung of a gluon proceeds via the final state radiation diagrams b) and c) depicted in Fig. 13. For this process, we calculate the double differential rate as

$$
\begin{aligned}
\frac{d^2\sigma_B^{\rm simp}}{dx_g dx_q} = &\frac{\alpha_s C_F \sigma_0^{\rm simp}}{4\pi\sqrt{1-\mu_q}} \\
&\times \frac{\mu_q x_g^2 + 2((1-x_g)^2 + 1)(1-x_g)(1-x_g-x_q)}{(1-x_q)^2(1-x_g-x_q)^2},
\end{aligned}
\tag{A8}
$$

which once integrated over the quark energy becomes

---

[8]These are diagrams containing gluinos, squark self-energies, and supersymmetric corrections to the quark self energy or the neutralino-squark–quark coupling. None of these diagrams lifts the helicity suppression of the tree-level annihilation.

[9]In the language of Ref. [28], this is simply the VIB part (while $\sigma_B^{\rm full}$ and $\sigma_B^{\rm simp}$ describes the full IB and FSR contributions, respectively).

$$\frac{d\sigma_B^{\text{simp}}}{dx_g} = \frac{2\alpha_s C_F \sigma_0^{\text{simp}}}{\pi x_g \sqrt{1-\mu_q}} \left[(1-\mu_q)\sqrt{(1-x_g)(1-x_g-\mu_q)} \right.$$
$$\left. - (1+(1-x_g)^2-\mu_q)\tanh^{-1}\sqrt{1-\frac{\mu_q}{1-x_g}} \right],$$
$$(A9)$$

where $x_g \equiv E_g/m_\chi$ and $\mu_q \equiv m_q^2/m_\chi^2$, and $C_F = 4/3$ is the $SU(3)$ Casimir operator associated to gluon emission from quarks. In the limit of small quark masses, $\mu_q \ll 1$, this reduces as expected to the well-known Weizsäcker-Williams expression [115,116]

$$\frac{d\sigma_B^{\text{simp}}}{dx_g} = \sigma_0^{\text{simp}} \frac{\alpha_s C_F}{\pi x_g} [1+(1-x_g)^2] \log \frac{4(1-x_g)}{\mu_q}. \tag{A10}$$

Note that the above result is model-independent in the sense that the parameters of the simplified-model Lagrangian (A1) do not explicitly enter in this expression. This changes when considering the full model because of VIB contributions, which can be traced back to the emission of gluons from t-channel squarks. In the language of the simplified model pseudoscalar ϕ, these processes generate three "anomalous" types of 4-point interactions given by dimension-5 and 6 operators, respectively[10]:

$$\mathcal{L}_{\text{VIB}}^{\text{simp}} = -\frac{1}{\Lambda_{p4}} \phi t_a A_a^\mu i \bar{q} \gamma^5 \overset{\leftrightarrow}{\partial_\mu} q - \frac{1}{\Lambda_{a4}^2} (\partial_\mu \phi) t_a A_a^\nu \bar{q} \overset{\leftrightarrow}{\partial_\nu} \gamma^\mu \gamma^5 q$$
$$- \frac{1}{\Lambda_{v4}^2} (\partial_\mu \phi) t_a A_a^\nu \bar{q} \overset{\leftrightarrow}{\partial_\nu} \gamma^\mu q, \tag{A11}$$

where t_a are the $SU(3)$ generators and A_a^μ the gluon fields. These operators thus arise in the zero velocity and quark-mass limit of the full theory, but are absent even at higher orders in the theory described by Eq. (A1) (recall that $g_p \propto m_q$); hence, they contribute to $\tilde{\sigma}_{\bar{q}qg}$ in Eq. (A7), but not to $\sigma_{\text{tot}}^{\text{simp}}$. This is a simple way of seeing how the helicity suppression of $\phi \to \bar{q}q$ can technically be lifted by gluon VIB.

To obtain the IB cross section in the full theory, which strongly depends on the choice of SUSY model, we use Eq. (2) to rescale the analytical solutions derived in Ref. [28]. As required by Kinoshita's and Bloch's theorems [117,118], the difference $(d\sigma_B^{\text{full}}/dx - d\sigma_B^{\text{simp}}/dx)$ is no longer IR divergent, nor divergent in the $\mu_q \to 0$ limit (see also the discussion in Appendix B). We can therefore

integrate it numerically to obtain the second term in our final result for the full cross section at leading order in α_s, Eq. (A5).

3. Pseudoscalar decay at NLO

The total NLO rate of quark production in the simplified model has contributions from the two operators in Eq. (A1), as well as from the gluon coupling to quarks. Being very similar to the decay of the scalar and pseudoscalar Higgs', we follow very closely the calculations of Refs. [119,120]. We thus have to consider the renormalized Lagrangian

$$\mathcal{L} = \bar{q}(i\slashed{D} - m_q)q - ig_p(1+\delta_p)\phi\bar{q}\gamma^5 q$$
$$- \frac{1+\delta_a}{\Lambda} \partial_\mu\phi\bar{q}\gamma^\mu\gamma^5 q. \tag{A12}$$

The counterterms δ_p and δ_a cancel the ultraviolet divergences from the vertex corrections in Fig. 13(d) to pseudoscalar and axial vector decays respectively. In the on shell renormalization scheme, they are given by

$$\delta_p = \delta_Z - \delta m/m_q + \delta_p^5,$$
$$\delta_a = \delta_Z + \delta_a^5, \tag{A13}$$

where m_q is the quark mass at the weak scale, and δ_Z and δ_m are the quark field rescaling counterterm and mass rescaling respectively. The terms $\delta_{p/a}^5$ renormalize the axial anomaly, that is, they take account of the fact that $\{\gamma^5, \gamma^\mu\} \neq 0$ in D dimensions and are required to maintain gauge invariance during the renormalization procedure [121]:

$$\delta_p^5 = -\frac{\alpha_s}{4\pi} 8C_F,$$
$$\delta_a^5 = -\frac{\alpha_s}{4\pi} 4C_F. \tag{A14}$$

Note that the axial vector coupling is nonrenormalizable, so the counterterm δ_a is an effective counterterm to cancel the divergence from the effective coupling; the Ward identity will ensure that a similar term proportional to the field rescaling will cancel the divergences in the full theory [122–125]. δm and δ_Z are derived from the quark self-energy, Fig. 14, and are given by
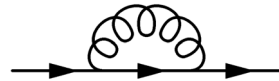

FIG. 14. 1-loop contribution to the quark self energy Σ.

---

[10]Technically, we consider the amplitude for the full $2 \to 3$ process and replace the initial state fermion bilinear with the projector P_{S_0}. All terms that survive in the $m_q \to 0$ limit then follow from the effective Lagrangian stated in Eq. (A11), with all coefficients $(\Lambda_{p4}, \Lambda_{a4}, \Lambda_{v4})$ uniquely defined by this procedure.

$$\frac{\delta m}{m_q} = \frac{\alpha_s C_F}{4\pi}\left[3\Gamma(\epsilon) - 3\log\left(\frac{\mu_q}{4\pi}\right) + 4\right],$$

$$\delta_Z \equiv Z_2 - 1$$

$$\simeq \frac{\alpha_s C_F}{4\pi}\left[-\Gamma(\epsilon) + 3\log\left(\frac{\mu_q}{4\pi}\right) - \log(\mu_g) - 4\right], \quad (A15)$$

where $D \equiv 4 - 2\epsilon$ to dimensionally regulate the UV divergence, and μ_g is a fictitious gluon mass (in units of m_χ^2) introduced to regulate the infrared (IR) divergence. We have omitted propagator counterterms in Eq. (A12), as their relevance only comes in at $\mathcal{O}(\alpha_s^2)$.

Real gluon emission from final state quark legs has already been discussed above and is described by Eq. (A9). The IR divergence of σ_B^{simp} is canceled by a corresponding divergence in $\sigma_V^{\text{simp}} + \sigma_C^{\text{simp}}$. Adding all processes discussed above leads to the total annihilation rate for the simplified model,

$$\sigma_{\text{tot}}^{\text{simp}} = \sigma_0^{\text{simp}} + \sigma_B^{\text{simp}} + \sigma_V^{\text{simp}} + \sigma_C^{\text{simp}}. \quad (A16)$$

In a different context, this has earlier been calculated by Drees and Hikasa [120]

$$\frac{\sigma_{\text{tot}}^{\text{simp}}}{\sigma_0^{\text{simp}}} = 1 + \frac{C_F \alpha_s}{\pi}\left[\frac{1+\beta_0^2}{\beta_0}\left(4\text{Li}_2\left(\frac{1-\beta_0}{1+\beta_0}\right)\right.\right.$$
$$+ 2\text{Li}_2\left(-\frac{1-\beta_0}{1+\beta_0}\right) - 3\log\frac{2}{1+\beta_0}\log\frac{1+\beta_0}{1-\beta_0}$$
$$\left.- 2\log\beta_0\log\frac{1+\beta_0}{1-\beta_0}\right) - 3\log\frac{4}{1-\beta_0^2} - 4\log\beta_0$$
$$\left.+ \frac{1}{16\beta_0}(19 + 2\beta_0^2 + 3\beta_0^4)\log\frac{1+\beta_0}{1-\beta_0} + \frac{3}{8}(7 - \beta_0^2)\right], \quad (A17)$$

where $\beta_0 \equiv \sqrt{1-\mu_q}$. We have verified that in the rest frame of the ϕ Eq. (A17) is true for both pseudoscalar and axial vector interactions. As Eq. (A17) approaches the quark threshold, $\beta_0 \to 0$, it diverges. This is a consequence of the color Coulomb interaction, and signifies the formation of bound states [126,127]. Very close to the threshold the above expression thus needs to be corrected which however is outside the scope of this work.

In the limit $\mu_q \to 0$ of small quark masses, relevant for models with large VIB enhancements, this reduces to

$$\sigma_{\text{tot}}^{\text{simp}} \simeq \sigma_0^{\text{simp}}\left[1 + \frac{3\alpha_s C_F}{4\pi}\left(3 + 2\log\frac{\mu_q}{4}\right)\right], \quad (A18)$$

a result which we derived independently and confirm. As required by Kinoshita's theorem [117] the unrenormalized rate must be free of mass divergences, thus the logarithmic divergence in Eq. (A18) comes from the counterterms in

Eq. (A12). For very small values of μ_q, this divergence indicates a breakdown in the reliability of the $\mathcal{O}(\alpha_s)$ calculation, and we are required to resum the leading log contributions to all orders in α_s. This results in replacing the leading log term in the above expression as [119,120]

$$\frac{6\alpha_s C_F}{\pi}\log\frac{\mu_q}{4} \to \left(\frac{\ln(4m_q^2/\Lambda_{\text{QCD}}^2)}{\ln(s/\Lambda_{\text{QCD}}^2)}\right)^{\frac{24}{33-2N_f}}, \quad (A19)$$

where N_f is the number of accessible quark flavors, and Λ_{QCD} is the QCD scale. This can be simplified further using the identity for the running quark mass, defined in the MS scheme

$$\frac{\bar{m}(\mu)}{\bar{m}(\mu_0)} = \left[\frac{\alpha_s(\mu)}{\alpha_s(\mu_0)}\right]^{\frac{2}{\pi b}} = \left[\frac{\ln(\mu_0/\Lambda_{\text{QCD}})}{\ln(\mu/\Lambda_{\text{QCD}})}\right]^{\frac{2}{\pi b}}, \quad (A20)$$

where $b = (33 - 2N_f)/(6\pi)$, and $\alpha_s(\mu)^{-1} \simeq b\ln(\sqrt{s}/\Lambda_{\text{QCD}})$ in the limit $\sqrt{s} \gg \Lambda_{\text{QCD}}$. Noting that *at zeroth order in α_s* the physical (pole) mass is equal to $m_q = \bar{m}(2m_q)$, we can see clearly that the effect of the resummation of leading logarithms coming from the renormalization procedure, equates to replacing g_p with a running Yukawa coupling. For consistency we also make this replacement in the tree level amplitude leaving us with a result that is both valid in the $\mu \to 0$ limit and interpolates with the full one-loop result (A16) [120]

$$\frac{\sigma_{\text{tot}}^{\text{simp}}}{\sigma_0^{\text{simp}}} \simeq \frac{\bar{m}^2(\sqrt{s})}{\bar{m}^2(2m_q)}\left[1 + \frac{9\alpha_s C_F}{4\pi}\right]. \quad (A21)$$

This expression constitutes the main result of Appendix A 3, so let us pause a moment to discuss it in more detail. For pseudoscalar processes the interpretation of this result is clear, we have simply rederived the running of the Yukawa interactions as in [119,120] The interpretation for the contribution from the axial vector interaction in Eq. (A1) is a little more subtle, but essentially boils down to the observation that only the timelike part of the axial vector coupling contributes to the decay of a pseudoscalar [because $p^\mu = (\sqrt{s}, \mathbf{0})$ in the rest frame of ϕ]; as this component has exactly the same transformation properties under rotations and mirror operations, we should expect to find the same results in both cases.[11] It is also worth to reflect about the overall normalization of Eq. (A21), which fixes the renormalization fix point for the running of the quark masses such that the tree-level result is recovered at

_____

[11]For an s-channel annihilation process mediated by a Z boson, there is also a more explicit way of seeing this. In the Landau gauge, e.g., it is straightforward to verify that the only contributing diagram is the one containing a massless Goldstone boson—which means that we actually have a Higgs propagator, just as in the case of the physical pseudoscalar A in the s-channel.

threshold, i.e. for $\sqrt{s} = 2m_q$. This appears—in hindsight, recall that we made no corresponding assumption during our derivation—to be the *only* possible energy scale at which one could sensibly require this to happen, simply because it is the only one that is available: the masses of virtual particles (such as the pseudoscalar A) only appear in a subset of relevant diagrams; and the neutralino pair is in some diagrams not even connected to the vertex to which we have calculated QCD corrections, hence the pseudoscalar mass $M = \sqrt{s} \simeq 2m_\chi$ is not a good alternative either. Let us stress that this situation is intrinsically different to the running of the Yukawa coupling y of the SM Higgs boson to fermions. In that case, a well-motivated (and in fact standard) renormalization fixpoint would be to require that the Higgs decay at rest corresponds to the one expected at tree level, which amounts to take into account the running by replacing $y_q \sim m_q$ with $y_q \sim \bar{m}(\sqrt{s})/\bar{m}(m_h)$.

The ratio (A21) of the QCD-corrected over tree-level cross section in the simplified model is shown in Fig. 15 for c, t and b quarks, where we have used the 4-loop results from Refs. [128,129] for the running MS quark masses (as implemented in DarkSUSY). The figure illustrates that the total cross section is significantly *suppressed* by QCD corrections for all quark final states across most of the parameter space, with the exception of top final states in the region close to the top threshold (though in the presence of substantial VIB contributions, not included in $\sigma_{\rm tot}^{\rm simp}$, the cross section will of course instead be *enhanced*, by a factor proportional to m_χ^2). For top final states, we show for comparison also the NLO result of Eq. (A17), which should be used for neutralino masses not much greater than the final state quark mass because the resummed expression (A21) is only valid for $m_q \gg m_\chi$. In practice, we implement
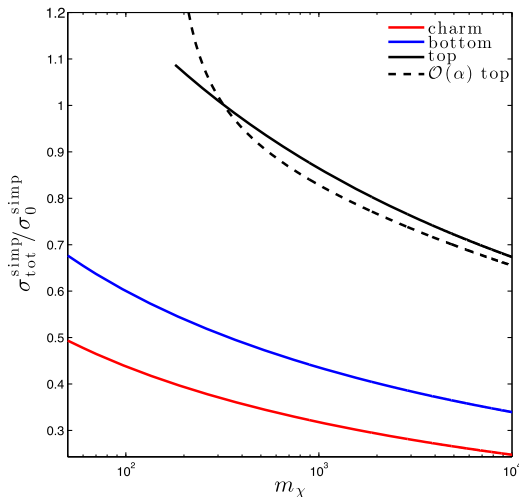

FIG. 15. Ratio of the total and tree level cross sections in the simplified model for $\bar{c}c$ (red), $\bar{b}b$ (blue), $\bar{t}t$ (black) quark final states (solid lines). For $\bar{t}t$, also NLO results are shown (dashed). All ratios use running $\alpha_s(2m_\chi)$.

a somewhat arbitrary ratio of $m_\chi/m_q = 1.85$ to divide between those two regimes (this is where the two lines in the figure cross).

We conclude this section by comparing our results with the way QCD corrections are currently implemented in DarkSUSY 5.1.2, which essentially amounts to including the effect of running quark masses solely in the Yukawa couplings that appear at tree-level (noting that micrOMEGAs [110] uses a very similar implementation). As discussed above, this incorrectly neglects the contribution from diagrams where the SM model Yukawa couplings do not enter explicitly, but which give an identical description in terms of our effective pseudoscalar model. To illustrate the size of this effect, we show in Fig. 16 the ratio of our improved result for $\sigma_{\rm tot}^{\rm simp}$ and the cross section $\sigma^{\rm DS}$ used in DarkSUSY for two specific situations: i) a pure Bino with the same characteristics as used in Sec. IV (left panel) and ii) a mixed neutralino in the "Higgs funnel" region with $m_A = 2m_\chi$ (right panel), chosen such that the annihilation rate is by far dominated by the exchange of a pseudoscalar Higgs in the s-channel. In the *Bino* case, the couplings that appear in annihilation diagrams have only subdominant Yukawa contributions (because we set the squark mixing to zero). Hence, $\sigma^{\rm DS}$ is as expected identical to the tree-level result, implying that the ratio $\sigma_{\rm tot}^{\rm simp}/\sigma^{\rm DS}$ is simply given by Eqs. (A17) and (A21) and hence Fig. 16. For the case of a *pseudoscalar mediator* in the s-channel, on the other hand, the origin of the leading correction factor in Eq. (A21) comes exclusively from the Yukawa coupling between A and final quark pair, and we might therefore expect exact agreement of our result with the DarkSUSY implementation. As visible in the figure, however, this is *not* the case. The reason for this discrepancy is that DarkSUSY 5.1.2 implements the Yukawa running *independently of the process under consideration* by replacing $m_q \to \bar{m}(2m_\chi)$ (as do many other numerical codes, including micrOMEGAs and, to some extent, DM@NLO). As discussed at length above, however, this corresponds to an unphysical renormalization condition for the specific process we are interested in here (i.e. the decay of an effective pseudoscalar particle with mass $M = \sqrt{s}$). Indeed, when artificially replacing $\bar{m}^2(2m_\chi)/\bar{m}^2(2m_q) \to \bar{m}^2(2m_\chi)/m_q^2$ in Eq. (A21), we find exact agreement as expected—up to the term $9C_F\alpha_s/4\pi$ which is not included in DarkSUSY. Numerically, the discrepancy between those two prescriptions is largest for light quarks.

As just illustrated, our corrected version of $\sigma_{\rm tot}^{\rm simp}$ can significantly affect predictions for the annihilation rate of a given SUSY model. We numerically implement it into DarkSUSY, alongside the difference $(\sigma_B^{\rm full} - \sigma_B^{\rm simp})$, thereby making both calculations of the relic density and present annihilation rates with this widely used tool significantly more reliable. The accuracy of neglecting the remaining term in Eq. (A5), $\sigma_{\rm Error}$, will be discussed below.
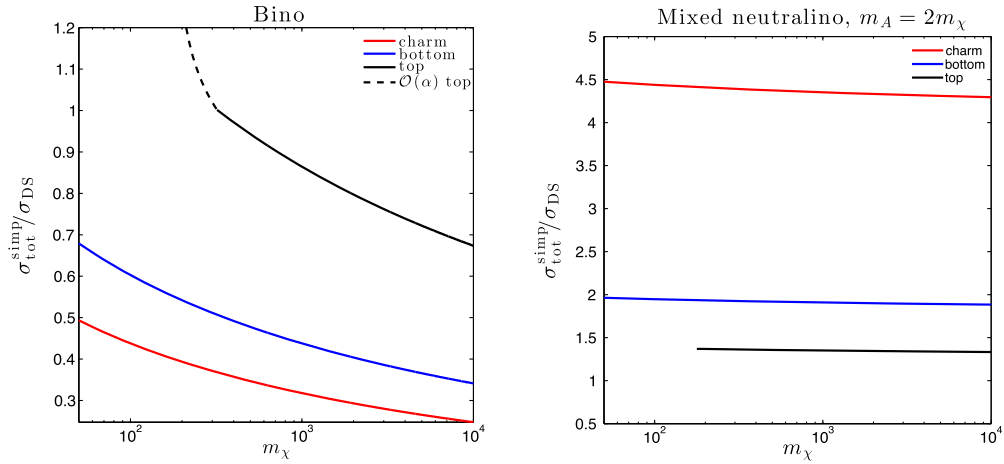
FIG. 16.   Ratio of our result for $\sigma_{\text{tot}}^{\text{simp}}$ and the annihilation cross section σ^{DS} as implemented in DarkSUSY 5.1.2. The various lines correspond to $\bar{c}c$ (red), $\bar{b}b$ (blue), $\bar{t}t$ (black) final states. *Left panel:* case of a pure Bino. *Right panel:* case of a mixed neutralino where annihilation via an *s*-channel pseudoscalar Higgs dominates. See text for a detailed discussion.

4. Expected error

The accuracy in treating dark matter annihilation as an effective decay at NLO is limited by the model dependent contribution σ_{Error}. As illustrated by Eq. (A6), this term has two contributions, the first is from the difference between the full theory and the simplified model, taking into account only final state gluon exchange graphs at NLO and appropriate counterterms. The second type of error, $\sigma_\star$, comes from neglected Feynman diagrams at the one loop level. Though the full calculation of these contributions is beyond the scope of this work, we can make an educated guess about their importance.

The *s*-channel Z and A mediated contributions to Fig. 4 have an identical vertex topology to axial vector and pseudoscalar decay processes, implying that for these diagrams the cancellations in Eq. (A6) are exact up to all orders in α_s. This is not the case for *t*-channel squark exchange as the *t*-channel propagator is a function of the off shell gluon momentum. Using simple power counting arguments, however, it is clear that the *t*-channel contribution to Fig. 4(a) is UV finite, negating the need for a counterterm for this diagram. However, to maintain gauge invariance we must add to this process *t*-channel graphs with $\mathcal{O}(\alpha_s)$ corrections to the neutralino-quark-squark vertex, which do indeed contain a UV divergence. As it turns out when neutralino-quark-squark vertex correction graphs are taken into account, the subtraction $(\sigma_V^{\text{full}} - \sigma_V^{\text{simp}})$ has no UV divergence, implying that in the term $(\sigma_C^{\text{full}} - \sigma_C^{\text{simp}})$ the cancellation of leading mass logarithms must also be exact. Similarly, when we add all $\mathcal{O}(\alpha_s)$ amplitude contributions including counterterms, we expect all IR divergences to cancel. One therefore expects some model-dependent error to enter in at $\mathcal{O}(\alpha_s)$, from in-exact *t*-channel cancellations in Eq. (A6), but that this error cannot contain large mass logarithms, and is therefore

expected to be small compared to Eq. (A21)—or the VIB contributions, $\sigma_B^{\text{full}} - \sigma_B^{\text{simp}}$, which dominate as several times stressed for $m_\chi \gg m_q$.

$\sigma_\star$ contains loops involving gluinos, squark self energy graphs, and supersymmetric corrections to the quark self energy. While the error from neglecting $\sigma_\star$ enters at $\mathcal{O}(\alpha_s)$ and in general is very model-dependent, we expect it not to be very sizable. The reason is that even though these additional diagrams potentially lead to large mass logarithms containing squark and gluino masses, those are typically not as large as the fully accounted-for logarithms containing quark masses in the $m_q \ll 2m_\chi$ limit (simply because the mass separation between supersymmetric states typically does not extend over several orders of magnitude). An exception to this general expectation are *b* quark final states where an extra source of error comes from sbottom-gluino and stop-chargino one-loop contributions to m_b, which can be substantial for large $\tan\beta$ or large A_b, and as such need to be resummed [54,130,131]. The result is a correction to the *b* mass which leads to an error in the simplified model cross section at zeroth order in α_s. While these unmodeled contributions to σ_{Error} are potentially worrisome, they are all helicity suppressed. Their importance thus diminishes when we consider models with large VIB $(\sigma_B^{\text{full}} - \sigma_B^{\text{simp}})$ contributions, the main interest of this work. From this discussion, we generally expect the biggest error in the cross section to come from neutralino annihilation into top quarks, for neutralino masses not too far above threshold.

To test the accuracy of our simplified model in this "critical regime", we compared the DarkSUSY result for the total neutralino cross section at NLO (σ_0^{simp} for $\chi\chi \to \bar{t}t$ & $\bar{t}tg$) with the full NLO result [55,112], which makes no simplifying assumptions and includes all $\mathcal{O}(\alpha_s)$ diagrams. Given differences in the treatment of the running

TABLE III. mSUGRA models with nonuniversal Higgs masses considered in Ref. [55]. The quantity Δ denotes the ratio of QCD-corrected to tree-level annihilation cross section to top quarks in the zero-velocity limit. The values obtained with the current version of DM@NLO [112] were kindly provided by B. Herrmann [132].

	m_0 [GeV]	M_2 [GeV]	A_0 [GeV]	$\tan\beta$	$\text{sign}(\mu)$	m_{H_u} [GeV]	m_{H_d} [GeV]	$m_{\tilde{\chi}_1^0}$	$m_{\tilde{t}}$	Δ_{full} [112] ([55])	Δ_{simp} [this work]	Diff. [%]
I	500	500	0	10	+	1500	1000	207.2	606.4	$-(1.22)$	1.22	< 1
II	620	580	0	10	+	1020	1020	223.7	923.8	1.32 (1.59)	1.15	−13
III	500	500	−1200	10	+	1250	2290	200.7	259.3	1.26 (1.22)	1.25	1

TABLE IV. As Table III, but for models in mSUGRA without gaugino mass unification.

	m_0 [GeV]	M_2 [GeV]	A_0 [GeV]	$\tan\beta$	$\text{sign}(\mu)$	$\frac{M_1}{M_2}$	$\frac{M_3}{M_2}$	$m_{\tilde{\chi}_1^0}$	$m_{\tilde{t}}$	Δ_{full} [112] ([55])	Δ_{simp} [this work]	Difference [%]
IV	300	700	−350	10	+	2/3	1/3	183.4	281.9	1.43 (1.25)	1.49	4
V	1500	600	0	10	+	1	4/9	235.6	939.0	1.34 (1.55)	1.12	−16

of SUSY parameters, the value of σ_0^{simp} calculated in DarkSUSY generally does not agree with the corresponding result in [55] at tree level. Therefore, to get a better representation of the error in our result, we only consider the fractional enhancement Δ of the zero velocity cross section at NLO over the tree level result. In Tables III and IV, we show this quantity for the models explicitly considered in Ref. [55]. Concretely, $\Delta_{\text{full}} \equiv \sigma_{\text{tot}}^{\text{full}}/\sigma_0$ represents the enhancement reported in [55], updated by using the latest version of DM@NLO [112], while $\Delta_{\text{simp}} \equiv \sigma_{\text{tot}}^{\text{simp}}/\sigma_0$ represents the enhancement within the simplified model discussed in this work.[12]

From this simple comparison the error in using the simplified model appears to be well below 20% for neutralino masses close to the top threshold. In some cases, like for model I, we find agreement with the full result to excellent precision. This is not altogether surprising given that in this model annihilation at tree level is dominated by A exchange, which only contributes to σ_{Error} at NLO through a gluino-squark loop diagram which is expected to be subdominant in comparison to the leading contributions. In models II and V annihilation at tree level is dominated by Z exchange. These constitute the worst agreement between the full theory and the simplified model, implying that the Z mediated gluino-squark loop process is important. In models III and IV annihilation at tree level is dominated by $\tilde{q}$ exchange and negative $Z/\tilde{q}$ interference terms. Thus the neglect of mixing terms

---

[12]Note that the DM@NLO package [112] presently cannot compute the cross section in the zero-velocity limit. For the sake of comparison, we thus use an *extrapolation* of the cross section obtained for small center-of-mass momenta. We are very grateful to B. Herrmann for providing these results [132].

between tree-level squark exchange and the Z mediated gluino-squark loop is a likely explanation for the—in fact not very sizeable—relative enhancement of the simplified model calculation over the full NLO result from DM@NLO [112,132].

We reiterate that the above comparison has focused on the most pessimistic case, as we expect the error in using the simplified model to be largest for close-to-threshold annihilation into $\bar{t}t$ pairs (because of the subdominance of $\bar{t}tg$ VIB relative to 2-body annihilation in this case). Given the advantages of our approach, in particular in terms of numerical performance, the agreement is thus actually surprisingly good. Let us also stress that the full NLO result [55] of course does not take into account leading logarithms from higher orders in α_s, which need to be resummed as they increase in importance. Far above threshold, for $m_\chi \gg m_q$, the result presented in Eq. (A21) can thus actually expected to provide a *more* accurate estimate of the annihilation rate than the full NLO result.

APPENDIX B: STABLE PARTICLE SPECTRA FROM NEUTRALINO ANNIHILATION

In Appendix A we have discussed in some detail how to approximate the full and differential cross section for the annihilation of two neutralinos in the framework of a simplified model that describes the decay of a pseudoscalar. We now turn to the computation of the spectrum of *stable* particles like photons or antiprotons that result from showering and fragmentation of the $\bar{q}q$ and $\bar{q}qg$ final states, again using the framework of our simplified model. The flux of these stable particles at source, i.e. before propagation in the Galactic halo, is conventionally written in the form $d\Phi/dT \propto \sigma_0^{\text{full}} dN/dT$. Here, $\sigma_0^{\text{full}} = \sigma_0^{\text{simp}}$ is the

tree-level annihilation cross section into $\bar{q}q$ and dN/dT is the differential number of antiprotons or photons *per tree-level annihilation*. Following from Eq. (A5), it is given by

$$\frac{dN}{dT} = \frac{\sigma_{\text{tot}}^{\text{simp}} + \sigma_{\text{Error}}}{\sigma_0^{\text{simp}}} \frac{dN_{\bar{q}q}}{dT} + \frac{\tilde{\sigma}_{\bar{q}qg}}{\sigma_0^{\text{simp}}} \frac{d\tilde{N}_{\bar{q}qg}}{dT}, \quad \text{(B1)}$$

where $\tilde{\sigma}_{\bar{q}qg} \equiv (\sigma_B^{\text{full}} - \sigma_B^{\text{simp}})$ and T is the kinetic energy of the stable particle in question. This spectrum is determined by four independent quantities which we will now discuss in more detail.

$\sigma_{\text{tot}}^{\text{simp}}$ and $\tilde{\sigma}_{\bar{q}qg}$ determine the normalization of the spectrum, and correspond to the simplified model and subtracted IB cross sections defined in Appendix A 1 (recall that we neglect the contribution from σ_{Error}, see discussion in Appendix A 4). They can be thought of as the normalizations of "2-body" and "3-body" spectra respectively, though in reality the simplified model cross section implicitly includes FSR contributions. Note in particular that using the *subtracted* IB cross section as a normalization for the 3-body part automatically ensures that there is no double-counting of processes already included in the 2-body part.

The $dN_{\bar{q}q}/dT$ is the differential number of antiprotons or gamma-rays per *total* annihilation for the simplified model and is the same as the result obtained by simulation of a 2-body $\bar{q}q$ final state in PYTHIA, including final state showering and hadronization. Given that the final state $\bar{q}q$ pair is produced back to back, the shape of this spectrum is only a function of m_χ and m_q. $d\tilde{N}_{\bar{q}qg}/dT$ on the other hand is what we call the *subtracted 3-body spectrum*. Explicitly

it is the differential number of antiprotons/gamma-rays per annihilation $\tilde{\sigma}_{\bar{q}qg}$, obtained after simulations of $\bar{q}qg$ final states in PYTHIA with a center of momentum energy of $2m_\chi$, randomly selecting 3-body kinematical distributions according to the probability distribution

$$\frac{d^2\tilde{N}_{\bar{q}qg}}{dx_g dx_q} \equiv \frac{1}{\tilde{\sigma}_{\bar{q}qg}} \left(\frac{d^2\sigma_B^{\text{full}}}{dx_g dx_q} - \frac{d^2\sigma_B^{\text{simp}}}{dx_g dx_q} \right). \quad \text{(B2)}$$

Here, we introduced dimensionless variables $x_g \equiv E_g/m_\chi$ and $x_q \equiv E_q/m_\chi$. By construction, this distribution is normalized to one after integration over the full phase space (though the integrand can be both positive and negative at a given point in phase space). In practice we select from the cumulative distribution function, which is an array between 0 and 1 with each element corresponding to steps in the integration of Eq. (B2), using a minimum resolution of $\Delta x_q = \Delta x_g = 10^{-3}$ (or 10^{-4} in cases where very small values of μ_f required a better resolution).

In general, $d\tilde{N}_{\bar{q}qg}/dT$ is highly dependent on SUSY model parameters, and should be determined on a model by model basis. It is however possible to define four extreme limits that bracket the range of possibilities with respect to the resulting spectrum in antiprotons and gamma rays. We refer to the *maximal VIB case* as the 3-body spectrum that deviates most strongly from the spectrum resulting from 2-body ($\bar{q}q$) final states. It results from the probability distribution that is obtained in the limit that the squark masses are exactly degenerate with the neutralino mass. We examine two extreme cases of this spectrum, firstly that of maximal squark mixing (which we define by $g_{\tilde{q}_i q\chi}^L = g_{\tilde{q}_i q\chi}^R$):

$$\frac{d^2\tilde{N}_{\bar{q}qg}^{\text{VIB,mix}}}{dx_q dx_g} \propto -\frac{8(x_q - 1)(x_g + x_q - 1)(\mu^2(x_g + 1) - 2\mu(x_g^2 + 4) - 4\sqrt{\mu}((x_g - 2)x_g + 2) - 2(x_g - 4)x_g)}{(\mu - 2x_q)^2(2(x_g + x_q - 2) + \mu)^2}$$

$$- \frac{2(x_g - 1)^2(2(\mu - 2)(5\mu + 8\sqrt{\mu} + 2)x_g + 4\mu^{5/2} - 24\mu^{3/2} + 3\mu^3 - 10\mu^2 - 16\mu + 16\sqrt{\mu} + 24)}{(\mu - 2x_q)^2(2(x_g + x_q - 2) + \mu)^2}$$

$$- \frac{2(\mu^3(9 - 2x_g) + 2\mu^2(9x_g - 19) + (64\mu - 24)(1 - x_g) + \sqrt{\mu}(16 - 32x_g) + 4\mu^{3/2}(\mu^2 - 3\mu + 2))}{(\mu - 2x_q)^2(2(x_g + x_q - 2) + \mu)^2}$$

$$- \frac{2(\sqrt{\mu} + 1)(\mu - 2)\sqrt{\mu}x_g^2(2x_g + \mu - 2)(-\mu(x_g - 2) + 2x_g + \mu^{3/2})}{(x_q - 1)(x_g + x_q - 1)(\mu - 2x_q)^2(2(x_g + x_q - 2) + \mu)^2} \quad \text{(B3)}$$

$$\rightarrow \frac{(4 - x_g)x_g}{(2 - x_g - x_q)x_q} \quad \text{for } \mu \rightarrow 0, \quad \text{(B4)}$$

and secondly the minimally mixed case (defined by $g_{\tilde{q}_L q\chi}^L = g_{\tilde{q}_R q\chi}^R = 0$):

$$\frac{d^2\tilde{N}_{\bar{q}qg}^{\text{VIB,mix}}}{dx_q dx_g} \propto \frac{8(x_q-1)(x_g+x_q-1)(\mu x_g^2+(1-x_g)(\mu^2-2\mu+4))}{(\mu-2x_q)^2(2(x_g+x_q-2)+\mu)^2}$$

$$-\frac{4(x_g-1)^2(\mu(\mu(3x_g+\mu-4)-8x_g)+4(x_g+1))}{(\mu-2x_q)^2(2(x_g+x_q-2)+\mu)^2} - \frac{4(\mu(\mu(x_g+\mu-4)-8x_g+8)+4(x_g-1))}{(\mu-2x_q)^2(2(x_g+x_q-2)+\mu)^2}$$

$$+\frac{(\mu-2)\mu x_g^2(\mu(x_g-2)-2x_g)(2x_q+\mu-2)}{(x_q-1)(x_g+x_q-1)(\mu-2x_q)^2(2(x_g+x_q-2)+\mu)^2} \tag{B5}$$

$$\rightarrow \frac{(1-x_g)((1-x_q)^2+(1-x_q-x_g)^2)}{x_g^2(2-x_g-x_q)^2} \quad \text{for } \mu \rightarrow 0. \tag{B6}$$

The 3-body spectrum that is *closest* to the spectrum from $\bar{q}q$ final states, on the other hand, is obtained in the limit of heavy squarks ($m_{\tilde{q}} \gg m_\chi$). This *heavy squark limit* can be thought of as the interference term arising from FSR and VIB contributions and takes a particularly simple form both for maximal squark mixing ($g_{\tilde{q}_i q\chi}^L = g_{\tilde{q}_i q\chi}^R$),

$$\frac{d^2\tilde{N}_{\bar{q}qg}^{m_{\tilde{q}}\rightarrow\infty,\text{mix}}}{dx_q dx_g} \propto 1 + \frac{\sqrt{\mu}x_g^3 - \mu x_g^2}{4(1-x_q)(x_g+x_q-1)}, \tag{B7}$$

and for vanishing squark mixings ($g_{\tilde{q}_L q\chi}^L = g_{\tilde{q}_R q\chi}^R = 0$),

$$\frac{d^2\tilde{N}_{\bar{q}qg}^{m_{\tilde{q}}\rightarrow\infty,\text{mix}}}{dx_q dx_g} \propto \frac{x_g^3}{(1-x_q)(x_g+x_q-1)}. \tag{B8}$$

Importantly the subtracted 3-body spectrum as defined in Eq. (B2) is always divergence free, with the IR and colinear divergences in the double differential rate $d^2N_B^{\text{full}}/dx_g dx_q$

canceled by the same divergence occurring in the simplified model. This is expected from the general discussion in Appendix A, but it is instructive to show this explicitly for the specific case of a maximal VIB spectrum as defined above. For this sake, we plot in Fig. 17 both the subtracted rate $d^2\tilde{N}_{\bar{q}qg}/dx_g dx_q$ and its unsubtracted analogue $d^2N_B^{\text{full}}/dx_g dx_q$, i.e. only the first term in Eq. (B2); in both cases we choose a $\bar{b}bg$ final state and a neutralino mass of 30 GeV. We also indicate in the figure the location of the divergences that result from the quark or squark propagators being on shell (blue dashed lines).

The unsubtracted rate clearly diverges on approaching the on shell conditions for the quark ($x_q + x_g = 1$) and antiquark ($x_q = 1$) propagators. This is the well-known colinear divergence, regulated by the small but nonzero quark mass that limits the available phase-space to $x_q < 1 - \frac{\mu x_g}{4(1-x_g)} + \mathcal{O}(\mu^2)$ and $x_q + x_g > 1 + \frac{\mu x_g}{4(1-x_g)} + \mathcal{O}(\mu^2)$. Also the standard infrared divergence for $x_g \rightarrow 0$ is clearly
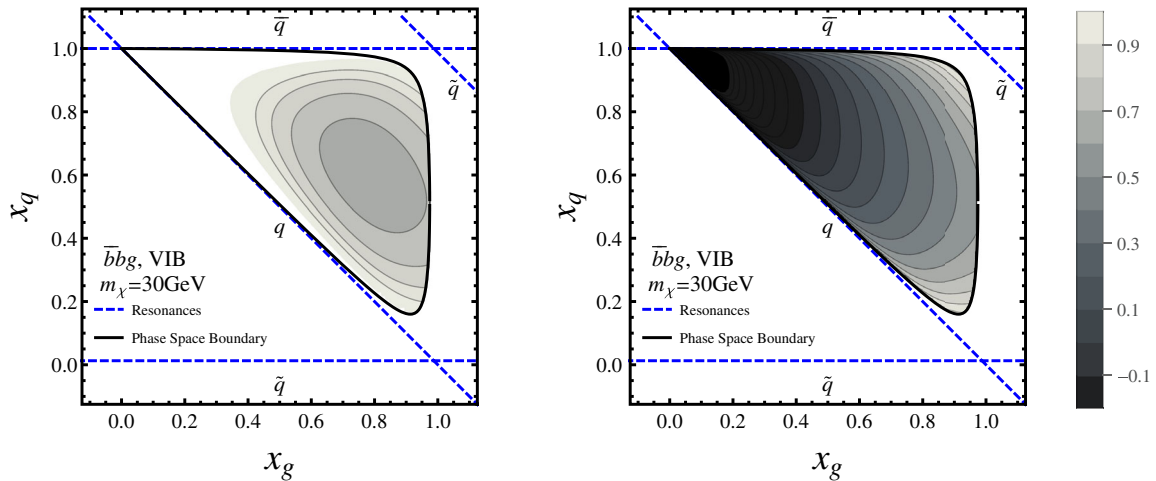

FIG. 17. Double differential annihilation rate within phase space boundary for neutralino annihilation into $\bar{b}bg$ for the full rate $d^2N_B^{\text{full}}/dx_g dx_q$ (*Left*) and the FSR subtracted rate $d^2\tilde{N}_{\bar{q}qg}/dx_g dx_q$ (*Right*), as defined in Eq. (B2). In both figures $m_\chi = 30$ GeV, and we assume a maximal VIB scenario ($g_{\tilde{q}q\chi}^L = g_{\tilde{q}q\chi}^R = 1$, $m_{\tilde{q}} = m_\chi$), the neutralino mass being chosen relatively low such as to demonstrate the effect of the quark mass on the shape of the phase-space boundary (solid line). The logarithmic color scale spans the range $-0.2 \leq \log_{10}(\frac{d^2N_B^{\text{full}}}{dx_g dx_q}) \leq 0.9$, white inside the solid line exceeds the upper bound in the range, and black exceeds the lower. Plotted alongside are the quark and squark resonances present in the diagrams.

visible (which can be regulated in a very similar way by introducing a fictitious gluon mass). On the other hand the subtracted rate $d\tilde{N}_{\bar{q}qg}/dx_g$ is finite over the whole region spanned by $\{x_q \leq 1\} \cap \{x_q + x_g \geq 1\} \cap \{x_g \leq 1\}$, dying completely off for infrared photons ($x_g \ll 1$). As a result, $d\tilde{N}_{\bar{q}qg}/dx_g$ now clearly peaks for large values of x_g, in particular when most of the remaining energy is carried by *either* q or $\bar{q}$. Note that this is different to the effect of the colinear divergences—which have been subtracted—and rather due to the presence of squark propagator resonances at $x_q = (3 - 2x_g - \mu_q + \mu_{\tilde{q}})/2$ and $x_q = (1 + \mu_q - \mu_{\tilde{q}})/2$, respectively. Obviously, this observation reinforces the naive interpretation of VIB being due to gluon emission from virtual squarks.

Phenomenologically, an on average larger gluon energy leads to a higher antiproton multiplicity. This can be explained by the fact that, due to its self-coupling, a high-energy gluon fragments more easily into high-energy partons than a high-energy quark. Indeed, we find that the antiproton spectrum that results from a pure VIB double-differential rate lies about halfway between that from $\bar{q}q$ and gg final states.[13] For $\mu_{\tilde{q}} \to \infty$, on the other hand, the squarks will decouple and the double-differential rate will no longer be strongly peaked towards $x_g \to 1$. As a result the spectrum will flatten and become more "3-bodylike", with the available energy being equally shared between all final states. We should thus naively expect that $\mu_{\tilde{q}} \to 1$ and $\mu_{\tilde{q}} \to \infty$ constitute the two limiting cases for the shape of both $d\tilde{N}_{\bar{q}qg}/dT$ and the resulting antiproton spectrum. These are the two limits used to fit the true model dependent spectrum, as discussed in the main text.

---

[13]For photons, in contrast, the difference is much smaller as they dominantly result from the decay of the much lighter neutral pions, which are copiously produced in particular by lower energy showers.

[1] J. Wess and B. Zumino, Nucl. Phys. **B70**, 39 (1974).
[2] P. Bechtle, K. Desch, H. K. Dreiner, M. Hamer, M. Krämer *et al.*, arXiv:1410.6035.
[3] O. Buchmueller, R. Cavanaugh, A. De Roeck, M. Dolan, J. Ellis *et al.*, Eur. Phys. J. C **74**, 2922 (2014).
[4] C. Strege, G. Bertone, G. J. Besjes, S. Caron, R. R. de Austri, A. Strubig, and R. Trotta, J. High Energy Phys. 09 (2014) 081.
[5] M. Cahill-Rowley, R. Cotta, A. Drlica-Wagner, S. Funk, J. Hewett, A. Ismail, T. Rizzo, and M. Wood, Phys. Rev. D **91**, 055011 (2015).
[6] L. Roszkowski, E. M. Sessolo, and A. J. Williams, J. High Energy Phys. 02 (2015) 014.
[7] K. J. de Vries *et al.*, Eur. Phys. J. C **75**, 422 (2015).
[8] G. Aad *et al.* (ATLAS Collaboration), J. High Energy Phys. 10 (2015) 134.
[9] P. Ade *et al.* (Planck Collaboration), arXiv:1502.01589.
[10] G. Jungman, M. Kamionkowski, and K. Griest, Phys. Rep. **267**, 195 (1996).
[11] G. Bertone, D. Hooper, and J. Silk, Phys. Rep. **405**, 279 (2005).
[12] D. Akerib *et al.* (LUX Collaboration), Phys. Rev. Lett. **112**, 091303 (2014).
[13] M. Ackermann *et al.* (Fermi-LAT Collaboration), Phys. Rev. Lett. **115**, 231301 (2015).
[14] L. Bergström, T. Bringmann, I. Cholis, D. Hooper, and C. Weniger, Phys. Rev. Lett. **111**, 171101 (2013).
[15] J. Edsjö and P. Gondolo, Phys. Rev. D **56**, 1879 (1997).
[16] J. R. Ellis, T. Falk, K. A. Olive, and M. Srednicki, Astropart. Phys. **13**, 181 (2000).
[17] K. Kawagoe and M. M. Nojiri, Phys. Rev. D **74**, 115011 (2006).
[18] A. Arbey, M. Battaglia, and F. Mahmoudi, arXiv:1506.02148.
[19] C. Boehm, A. Djouadi, and Y. Mambrini, Phys. Rev. D **61**, 095006 (2000).
[20] P. Agrawal and C. Frugiuele, J. High Energy Phys. 01 (2014) 115.
[21] M. Blanke, G. F. Giudice, P. Paradisi, G. Perez, and J. Zupan, J. High Energy Phys. 06 (2013) 022.
[22] J. Hisano, K. Ishiwata, and N. Nagata, Phys. Lett. B **706**, 208 (2011).
[23] M. Garny, A. Ibarra, M. Pato, and S. Vogl, J. Cosmol. Astropart. Phys. 11 (2012) 017.
[24] M. Asano, T. Bringmann, and C. Weniger, Phys. Lett. B **709**, 128 (2012).
[25] T. J. Weiler, AIP Conf. Proc. **1534**, 165 (2013).
[26] L. Bergström, Phys. Lett. B **225**, 372 (1989).
[27] R. Flores, K. A. Olive, and S. Rudaz, Phys. Lett. B **232**, 377 (1989).
[28] T. Bringmann, L. Bergström, and J. Edsjö, J. High Energy Phys. 01 (2008) 049.
[29] L. Bergström, T. Bringmann, and J. Edsjö, Phys. Rev. D **78**, 103520 (2008).
[30] E. Baltz and L. Bergström, Phys. Rev. D **67**, 043516 (2003).
[31] J. F. Beacom, N. F. Bell, and G. Bertone, Phys. Rev. Lett. **94**, 171301 (2005).
[32] N. F. Bell and T. D. Jacques, Phys. Rev. D **79**, 043507 (2009).
[33] V. Barger, Y. Gao, W. Y. Keung, and D. Marfatia, Phys. Rev. D **80**, 063537 (2009).
[34] T. Bringmann, X. Huang, A. Ibarra, S. Vogl, and C. Weniger, J. Cosmol. Astropart. Phys. 07 (2012) 054
[35] L. Bergström, Phys. Rev. D **86**, 103514 (2012).

[36] M. Garny, A. Ibarra, M. Pato, and S. Vogl, J. Cosmol. Astropart. Phys. 12 (2013) 046.

[37] T. Toma, Phys. Rev. Lett. 111, 091301 (2013).

[38] F. Giacchino, L. Lopez-Honorez, and M. H. Tytgat, J. Cosmol. Astropart. Phys. 10 (2013) 025.

[39] M. Kachelriess, P. D. Serpico, and M. A. Solberg, Phys. Rev. D 80, 123533 (2009).

[40] N. F. Bell, J. B. Dent, T. D. Jacques, and T. J. Weiler, Phys. Rev. D 83, 013001 (2011).

[41] C. E. Yaguna, Phys. Rev. D 81, 075024 (2010).

[42] N. F. Bell, J. B. Dent, T. D. Jacques, and T. J. Weiler, Phys. Rev. D 84, 103517 (2011).

[43] P. Ciafaloni, M. Cirelli, D. Comelli, A. De Simone, A. Riotto, and A. Urbano, J. Cosmol. Astropart. Phys. 06 (2011) 018.

[44] N. F. Bell, J. B. Dent, A. J. Galea, T. D. Jacques, L. M. Krauss, and T. J. Weiler, Phys. Lett. B 706, 6 (2011).

[45] M. Garny, A. Ibarra, and S. Vogl, J. Cosmol. Astropart. Phys. 07 (2011) 028.

[46] P. Ciafaloni, M. Cirelli, D. Comelli, A. De Simone, A. Riotto, and A. Urbano, J. Cosmol. Astropart. Phys. 10 (2011) 034.

[47] P. Ciafaloni, D. Comelli, A. De Simone, A. Riotto, and A. Urbano, J. Cosmol. Astropart. Phys. 06 (2012) 016.

[48] K. Fukushima, Y. Gao, J. Kumar, and D. Marfatia, Phys. Rev. D 86, 076014 (2012).

[49] N. F. Bell, A. J. Brennan, and T. D. Jacques, J. Cosmol. Astropart. Phys. 10 (2012) 045.

[50] T. Bringmann and F. Calore, Phys. Rev. Lett. 112, 071301 (2014).

[51] M. Drees, G. Jungman, M. Kamionkowski, and M. M. Nojiri, Phys. Rev. D 49, 636 (1994).

[52] M. Garny, A. Ibarra, and S. Vogl, J. Cosmol. Astropart. Phys. 04 (2012) 033.

[53] P. Gondolo, J. Edsjo, P. Ullio, L. Bergstrom, M. Schelke, and E. A. Baltz, J. Cosmol. Astropart. Phys. 07 (2004) 008; P. Gondolo, E. Edsjö, P. Ullio, L. Bergström, M. Schelke, E. A. Baltz, T. Bringmann, and G. Duda, http://www.darksusy.org.

[54] B. Herrmann and M. Klasen, Phys. Rev. D 76, 117704 (2007).

[55] B. Herrmann, M. Klasen, and K. Kovařik, Phys. Rev. D 80, 085025 (2009).

[56] B. Herrmann, M. Klasen, and K. Kovarik, Phys. Rev. D 79, 061701 (2009).

[57] B. Herrmann, M. Klasen, K. Kovarik, M. Meinecke, and P. Steppeler, Phys. Rev. D 89, 114012 (2014).

[58] T. Bringmann and C. Weniger, Phys. Dark Univ. 1, 194 (2012).

[59] T. Sjöstrand, S. Mrenna, and P. Z. Skands, Comput. Phys. Commun. 178, 852 (2008).

[60] T. Sjostrand, S. Mrenna, and P. Z. Skands, J. High Energy Phys. 05 (2006) 026.

[61] V. L. Ginzburg and S. I. Syrovatskii, The Origin of Cosmic Rays (Macmillan, New York, 1964).

[62] T. Bringmann, M. Vollmann, and C. Weniger, Phys. Rev. D 90, 123001 (2014).

[63] L. Gleeson and W. Axford, Astrophys. J. 154, 1011 (1968).

[64] J. S. Perko, Astron. Astrophys. 184, 119 (1987).

[65] T. Bringmann and P. Salati, Phys. Rev. D 75, 083006 (2007).

[66] F. Donato, D. Maurin, P. Salati, A. Barrau, G. Boudoul, and R. Taillet, Astrophys. J. 563, 172 (2001).

[67] C. Evoli, I. Cholis, D. Grasso, L. Maccione, and P. Ullio, Phys. Rev. D 85, 123511 (2012).

[68] W. A. Rolke, A. M. Lopez, and J. Conrad, Nucl. Instrum. Methods Phys. Res., Sect. A 551, 493 (2005).

[69] O. Adriani et al., Pis'ma Zh. Eksp. Teor. Fiz. 96, 693 (2012) [JETP Lett. 96, 621 (2013)].

[70] AMS-02 Collaboration, AMS Days at CERN, 2015, http://indico.cern.ch/event/381134/.

[71] P. Achard et al. (L3 Collaboration), Phys. Lett. B 580, 37 (2004).

[72] L. S. W. Group, ALEPH, DELPHI, L3, OPAL Experiments, LEPSUSYWG/04-02.1, http://lepsusy.web.cern.ch/lepsusy/www/squarks_summer04/stop_combi_208_final.html.

[73] G. Aad et al. (ATLAS Collaboration), J. High Energy Phys. 09 (2014) 176.

[74] G. Aad et al. (ATLAS Collaboration), Eur. Phys. J. C 75, 510 (2015).

[75] L. Bergstrom and H. Snellman, Phys. Rev. D 37, 3737 (1988).

[76] F. Donato, N. Fornengo, D. Maurin, and P. Salati, Phys. Rev. D 69, 063501 (2004).

[77] G. Aad et al. (ATLAS Collaboration), J. High Energy Phys. 10 (2015) 054.

[78] S. Chatrchyan et al. (CMS Collaboration), J. High Energy Phys. 06 (2014) 055.

[79] K. A. Olive et al. (Particle Data Group Collaboration), Chin. Phys. C 38, 090001 (2014).

[80] W. B. Atwood et al. (Fermi-LAT Collaboration), Astrophys. J. 697, 1071 (2009).

[81] P. Gondolo and G. Gelmini, Nucl. Phys. B360, 145 (1991).

[82] J. Hisano, S. Matsumoto, M. Nagai, O. Saito, and M. Senami, Phys. Lett. B 646, 34 (2007)

[83] A. Hryczuk, R. Iengo, and P. Ullio, J. High Energy Phys. 03 (2011) 069.

[84] A. Hryczuk, Phys. Lett. B 699, 271 (2011).

[85] A. Freitas, Phys. Lett. B 652, 280 (2007).

[86] K. Kovarik and B. Herrmann, AIP Conf. Proc. 1200, 1075 (2010).

[87] F. Boudjema, G. D. La Rochelle, and S. Kulkarni, Phys. Rev. D 84, 116001 (2011).

[88] A. Chatterjee, M. Drees, and S. Kulkarni, Phys. Rev. D 86, 105025 (2012).

[89] S. P. Martin, Adv. Ser. Dir. High Energy Phys. 21, 1 (2010).

[90] Q. L. BoulcH, Ph.D. thesis, Université de Grenoble, 2013.

[91] C. Boehm, A. Djouadi, and M. Drees, Phys. Rev. D 62, 035012 (2000).

[92] J. R. Ellis, K. A. Olive, and Y. Santoso, Astropart. Phys. 18, 395 (2003).

[93] V. Bednyakov, H. Klapdor-Kleingrothaus, and V. Gronewold, Phys. Rev. D 66, 115005 (2002).

[94] Y. Santoso, Nucl. Phys. B, Proc. Suppl. 124, 166 (2003).

[95] H. Baer, C. Balazs, and A. Belyaev, J. High Energy Phys. 03 (2002) 042.

[96] J. Edsjo, M. Schelke, P. Ullio, and P. Gondolo, J. Cosmol. Astropart. Phys. 04 (2003) 001.

[97] M. A. Ajaib, T. Li, and Q. Shafi, Phys. Rev. D 85, 055021 (2012).

[98] J. L. Diaz-Cruz, J. R. Ellis, K. A. Olive, and Y. Santoso, J. High Energy Phys. 05 (2007) 003.

[99] K. Huitu, L. Leinonen, and J. Laamanen, Phys. Rev. D 84, 075021 (2011).

[100] J. Ellis, K. A. Olive, and J. Zheng, Eur. Phys. J. C 74, 2947 (2014).

[101] A. Ibarra, A. Pierce, N. Shah, and S. Vogl, Phys. Rev. D 91, 095018 (2015).

[102] G. Aad et al. (ATLAS Collaboration), Phys. Lett. B 716, 1 (2012).

[103] S. Chatrchyan et al. (CMS Collaboration), Phys. Lett. B 716, 30 (2012).

[104] C. Balazs, M. Carena, and C. E. M. Wagner, Phys. Rev. D 70, 015007 (2004).

[105] J. Harz, B. Herrmann, M. Klasen, K. Kovarik, and Q. L. Boulc'h, Phys. Rev. D 87, 054031 (2013).

[106] J. Harz, PhD thesis, Report No. DESY-THESIS-2013-048, 2013.

[107] J. Harz, B. Herrmann, M. Klasen, K. Kovarik, and Q. Le Boulc'h, Proc. Sci., Corfu2012 (2013) 075, arXiv: 1302.3525.

[108] J. Harz, B. Herrmann, M. Klasen, K. Kovak, and M. Meinecke, Phys. Rev. D 91, 034012 (2015).

[109] J. Harz, B. Herrmann, M. Klasen, and K. Kovarik, Phys. Rev. D 91, 034028 (2015).

[110] G. Belanger, F. Boudjema, A. Pukhov, and A. Semenov, Comput. Phys. Commun. 185, 960 (2014).

[111] T. Bringmann, F. Calore, A. Galea, and M. Garny (to be published).

[112] http://dmnlo.hepforge.org.

[113] F. James and M. Roos, Comput. Phys. Commun. 10, 343 (1975).

[114] F. Calore, Ph.D. thesis, Hamburg, 2013.

[115] L. Bergström, T. Bringmann, M. Eriksson, and M. Gustafsson, Phys. Rev. Lett. 94, 131301 (2005).

[116] A. Birkedal, K. T. Matchev, M. Perelstein, and A. Spray, arXiv:hep-ph/0507194.

[117] T. Kinoshita, J. Math. Phys. 3, 650 (1962).

[118] F. Bloch and A. Nordsieck, Phys. Rev. 52, 54 (1937).

[119] E. Braaten and J. Leveille, Phys. Rev. D 22, 715 (1980).

[120] M. Drees and K. Hikasa, Phys. Lett. B 240, 455 (1990).

[121] S. Larin, Phys. Lett. B 303, 113 (1993).

[122] F. A. Berends, K. Gaemer, and R. Gastmans, Nucl. Phys. B57, 381 (1973).

[123] F. A. Berends, R. Kleiss, S. Jadach, and Z. Was, Acta Phys. Pol. B 14, 413 (1983).

[124] A. Akhundov, D. Y. Bardin, O. Fedorenko, and T. Riemann, Sov. J. Nucl. Phys. 42, 762 (1985).

[125] M. E. Peskin and D. V. Schroeder, An Introduction to Quantum Field Theory (Addison-Wesley, Reading, 1995), p. 842.

[126] M. Drees and K.-i. Hikasa, Phys. Rev. D 41, 1547 (1990).

[127] L. Reinders, H. Rubinstein, and S. Yazaki, Phys. Lett. 94B, 203 (1980).

[128] K. Chetyrkin and J. H. Kühn, Phys. Lett. B 248, 359 (1990).

[129] K. Chetyrkin, J. H. Kuhn, and M. Steinhauser, Comput. Phys. Commun. 133, 43 (2000).

[130] M. Carena, D. Garcia, U. Nierste, and C. E. Wagner, Nucl. Phys. B577, 88 (2000).

[131] J. Guasch, P. Häfliger, and M. Spira, Phys. Rev. D 68, 115001 (2003).

[132] B. Herrmann (private communication).